Advanced Powder Technology 33 (2022) 103836

Contents lists available at ScienceDirect

Advanced Powder Technology

journal homepage: www.elsevier.com/locate/apt

A concise treatise on model-based enhancements of cohesive powder properties via dry particle coating

Rajesh Davé *, Sangah Kim, Kuriakose Kunnath, Siddharth Tripathi

New Jersey Center for Engineered Particulates (NJCEP), New Jersey Institute of Technology, Newark, NJ 07102, USA

ARTICLE INFO

Article history:
Received 31 July 2022
Received in revised form 29 September 2022
Accepted 6 October 2022

Keywords:
Cohesive powder property enhancements
van der Waals forces
Particle contact models
Dry coating
Pharmaceutical blends

ABSTRACT

This paper presents a review of our key advances in model-guided dry coating-based enhancements of poor flow and packing of fine cohesive powders. The existing van der Waals force-based particle-contact models are reviewed to elucidate the main mechanism of flow enhancement through silica dry coating. Our multi-asperity model explains the effect of the amount of silica, insufficient flowability enhancements through conventional blending, and the predominant effect of particle surface roughness on cohesion reduction. Models are presented for the determination of the amount and type of guest particles, and estimation of the granular Bond number, used for cohesion nondimensionalization, based on particle size, particle density, asperity size, surface area coverage, and dispersive surface energy. Selection of the processing conditions for LabRAM, a benchmarking device, is presented followed by key examples of enhancements of flow, packing, agglomeration, and dissolution through the dry coating. Powder agglomeration is shown as a screening indicator of powder flowability. The mixing synergy is identified as a cause for enhanced blend flowability with a minor dry coated constituent at silica < 0.01%. The analysis and outcomes presented in this paper are intended to demonstrate the importance of dry coating as an essential tool for industry practitioners.

Contents

1. Introduction . . . 2
2. Theory . . . 4
   2.1. Particle contact models . . . 4
   2.2. Estimation of silica amount and type: Guest-host compatibility . . . 6
   2.3. Estimation of nondimensional cohesion via the granular Bond number . . . 8
   2.4. Bulk powder flowability assessments . . . 10
3. Experimental . . . 10
   3.1. Dry coating devices and LabRAM as a material sparing benchmarking device . . . 10
   3.2. LabRAM-based dry coating for mitigating flow, packing, agglomeration, and dissolution problems with pharmaceutical powders . . . 11
   3.3. Enhancement of blend properties for enabling direct compression tableting: Mixing synergy due to one dry coated component . . . 13
4. Summary and future work/forward outlook . . . 17
   Declaration of Competing Interest . . . 18
   Acknowledgements . . . 18
   Funding . . . 18
   References . . . 18

* Corresponding author.
E-mail address: dave@njit.edu (R. Davé).

https://doi.org/10.1016/j.apt.2022.103836

1. Introduction

Fine powders are cohesive unless they are specifically engineered to have reduced cohesion and improved flow, packing and dispersibility, for example, pharmaceutical powders with significantly enhanced flowability and bulk density after dry coating [1-17]. Generally, smaller the particle, poorer its flow, see for example all particles under 30 μm sized active pharmaceutical ingredients (APIs) and excipients in Table 1 (note that suggested FFC based flow regimes are: FFC < 2 – *very cohesive*, 2 < FFC < 4 – *cohesive*, 4 < FFC < 10 – *easy flowing*, and FFC > 10 – *free flowing*) [18]. The flowability of powders is expressed through FFC in this work. However, it could also be described using other indices such as Carr index, Hausner ratio, orifice meter, or the angle of repose (AoR) [5,19,20]. The flowability regimes as per FFC, indicated using the shading scheme in Table 1, suggest that the particle size has a predominant influence. That trend is confirmed in Fig. 1. Such trends are also evident for powder bulk density (BD), another strong indicator of powder cohesion [14,21,22]. However, as was shown previously, unlike FFC, the bulk density as a function of particle size has a significant scatter [14,21].

In addition to the median particle size, the powder cohesion, flowability, and bulk density are also influenced by many other factors such as the particle material, size distribution, shape, morphology, surface roughness, surface energy, as well as environmental conditions, e.g., the relative humidity and temperature [14,17,23-26]. Powder cohesion is a result of various particle interaction forces, including but not limited to van der Waals (vdW), electrostatic, liquid bridge, etc. It is useful to clarify that the term cohesion is relative because a common statement like "smaller powders are more cohesive" is incorrect since cohesive forces, e.g., vdW or liquid bridge are a function of the particle size, hence smaller particle size means smaller force magnitudes. The correct interpretation is that the cohesion force for smaller particles is larger as compared to a relevant body force, e.g., particle weight, buoyancy force, drag force, etc. Quantitatively, while the cohesion scales to particle radius r, the weight scales to r^3. To better understand the relative cohesion, it is useful to consider the granular Bond number, Bo_g, defined as the ratio of the sum of cohesive forces to the body forces. For dry, uncharged powders, it is essentially the ratio of particle–particle vdW force to particle weight [21,24,27-30]. Generally, when $Bo_g \leq 1$, particles are non-cohesive and free flowing, and when $Bo_g \gg 1$, they are cohesive and poorly flowing. Strictly speaking, perfectly smooth spherical particles $\leq$ 100 μm have $Bo_g > 1$ and hence they would flow poorly. Fortunately, most powders are micro rough as was discovered while examining the fluidization behavior of ~ 100 μm fluidized-bed catalytic cracking (FCC) particles and hence they have reduced cohesion as compared to perfectly smooth particles of the same size [31]. While even 70–150 μm particles could exhibit good flow due to their natural roughness, finer powders, e.g., 30 μm and smaller are poorly flowing despite natural surface asperities.

An attractive approach to tackle the poor flowability of fine powders is dry coating, a liquid-free, environmentally benign method for reducing the cohesion of fine powders, leading to improved bulk powder properties, e.g., the flowability, packing

Table 1
The sizes, FFC values, and flow regime of the API and excipient powders referenced in this paper. The powders are grouped by their flow regime, in the order of increasing $d_{3,2}$ within each flow category. FFC based flow regimes are: FFC < 2 – very cohesive, 2 < FFC < 4 – cohesive, 4 < FFC < 10 – easy flowing, and FFC > 10 – free flowing.

Material	d_{50} (μm)	$d_{3,2}$ (μm)	FFC	Flow Regime
Inhalac500	4.2	2.6	1.8	Very cohesive
Inhalac400	9.6	4.2	1.5	
Sorbolac 400 (Sorb400)	8.7	4.3	1.5	
Fenofibrate (FNB)	6.8	4.5	1.4	
micronized Acetaminophen (mAPAP)	7.3	4.8	1.2	
Ibuprofen milled to 5 microns (Ibu5)	6.0	5.1	1.1	
Ibuprofen milled to 10 microns (Ibu10)	10.7	7.0	1.1	
Pharmatose 450 (Pharm450)	19.2	17.0	1.9	
Itraconazole (ITZ)	10.0	5.3	2.1	Cohesive
Griseofulvin (GF)	10.6	6.4	2.9	
Granulac 230 (Gran230)	22.0	7.4	2.3	
Granulac 200 (Gran200)	27.9	10.3	2.5	
Avicel 105 (Av105)	19.0	10.8	2.4	
Ibuprofen milled to 20 microns (Ibu20)	21.6	11.2	3.4	
Cornstarch (CS)	14.4	15.0	3.7	
coarse Acetaminophen (cAPAP)	23.3	17.5	2.7	
Pharmatose 350 (Pharm350)	28.3	26.0	2.4	
Ibuprofen 70 (IBU70)	65.0	20.5	6.2	Easy Flowing
Ibuprofen 50 (Ibu50)	52.8	32.2	4.3	
Lactose 120 (Lac120)	93.9	38.9	6.6	
Avicel 101 (Av101)	64.2	42.9	7.4	
Theophylline (THPY)	137.0	74.3	7.7	
Avicel 102 (Av102)	116.6	66.0	12.1	Free Flowing
Pharmatose DCL11 (DCL11)	115.4	85.2	13.4	
Avicel 200 (Av200)	185.9	100.4	11.0	
Ascorbic Acid (AA)	224.3	123.4	10.2	

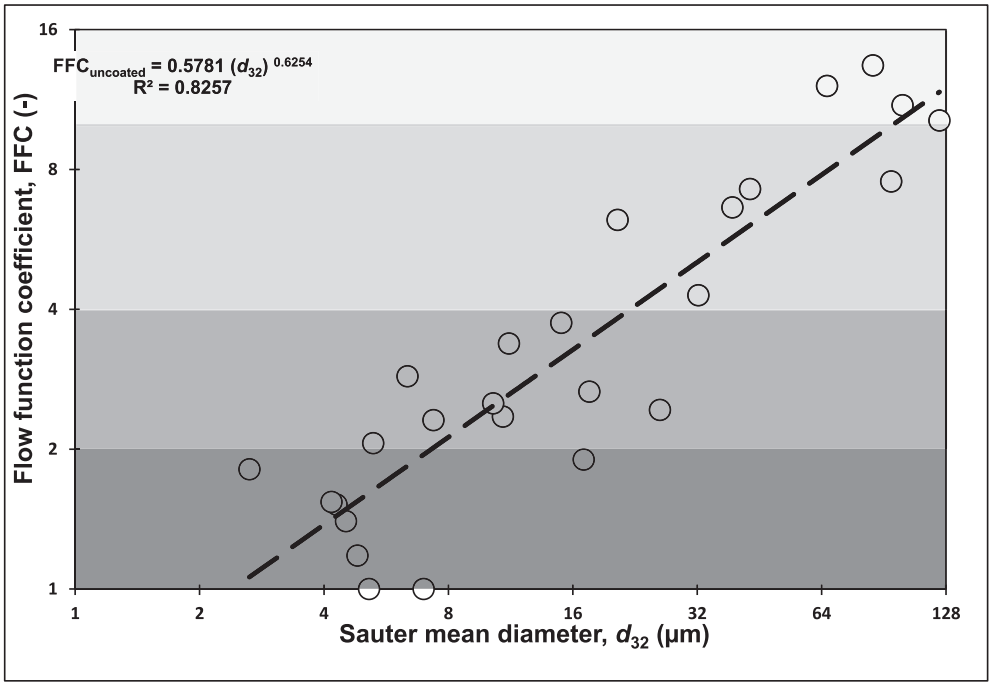

Fig. 1. Flowability (FFC) of 26 pharmaceutical powder materials of Table 1, plotted as a function of their Sauter mean diameter, in log–log (base 2) plot. A power law trend line appears to capture the trend although there is significant scatter.

density, agglomeration, fluidization, and dissolution [4,8,32-34]. In dry coating, fine cohesive powders (host particles), and flow aids such as nano-silica, which are an order of magnitude smaller (guest particles), are mixed at high intensity, instead of conventional mixing devices to uniformly distribute the guest particles onto the host particles [32]. The main mechanism of reduced cohesion from dry coating is the superimposition of nano-scale surface roughness arising from uniformly coated nano-size guest particles [32,33,35-38]. In ***Section 2***, these vdW-based contact models and their essential features are discussed further to confirm the main mechanism of flowability enhancement due to dry coating and highlight particle-scale *tuning* parameters that govern particle cohesion, hence flowability. The commonality between various traditional contact models [32,35-42], considered single-asperity models, and their short-comings as compared to the multi-asperity models [33,43,44] are also presented. Additional relevant material on such topics may be found in various key papers and review articles, including the one on capillary forces [40,42,45-50]. Last, theoretical background along with illustrative examples are provided to guide the selection of the ideal type, amount, and size of the guest particles, including testing guest–host compatibility.

Section 2 also lays the foundation for nondimensionalization of particle cohesion via Bond number, needed to capture key factors such as the surface roughness, surface energy, particle morphology, shape, and size distribution, all of which influence cohesion and flowability. Next, particle-scale measurements, needed to estimate the Bond number, are discussed along with pertinent equations. Bond number based nondimensionalization also helps in linking particle-scale properties to bulk-scale properties, such as powder bulk density or packing porosity [21,28], minimum bubbling velocity in fluidization (See power-law relationship in Figure 17 in [44], and powder flowability (see Fig. 6 in [24]) [30]. This section is concluded with a brief discussion of shear testing and evaluation of the flow function coefficient (FFC).

Section 3 presents an overview of dry coating devices, both conventional and emerging, which are essentially high-intensity mixing devices, such as the mechanofusion, the hybridizer, magnetically assisted impaction coating (MAIC), and recently developed devices in our group such as the fluid energy mill (FEM), the conical screen mill (comil), and a high-intensity vibration device called the LabRAM [5,6,8-10,51-53]. Such devices differ in terms of their mode of operation, either batch-mode or continuous-mode, and in terms of their potential for wide-scale industrial applicability, the determination of the latter would be a topic of future investigation. In our group, MAIC has been previously used as a lab-scale, batch-mode benchmarking device. However, now LabRAM is used in the same manner to provide a preliminary assessment of the extent of flowability enhancement or effectiveness of dry coating for the host and guest material pairs of interest. This section also presents a limited investigation of the selection of typical operating parameters for LabRAM and provide comparative results of LabRAM and MAIC outcomes for several API and excipients powders; note that the selection of MAIC operating parameters has been reported previously [4]. Key examples are presented to demonstrate the use of LabRAM-based dry coating for mitigating flow, packing, agglomeration, and dissolution problems with pharmaceutical powders. Another significant advantage of dry coating is the enhanced blend properties as well as the potential for direct compression tableting even when only one constituent of the blend is dry coated [34,52,54-56]. Several illustrative case studies of improved blend properties when one of the components of blends, which could also be a fine excipient, is dry coated are presented to convey the potential impact dry coating.

The last section (***Section 4***) presents a summary of key advances and industrially relevant model-based guidelines for enhancements of cohesive powder properties via dry coating based particle surface engineering. The major challenges along with the opportunities for further research are outlined. Notwithstanding the limited scope of the present paper and using examples almost exclusively from the pharmaceutical industry, it is expected that the outcomes and guidelines provided are general enough for all industries dealing with fine cohesive powders used in their respective applications.

2. Theory

2.1. Particle contact models

Pioneering work towards understanding the vdW forces between "rough" spheres involved examining the significance of the presence of small asperities on the powder surfaces [35], where Rumpf considered a single hemispherical asperity and derived the contact forces using vdW interaction model. In the Rumpf model, shown in Eq. (1), the first term represents the interaction of the large sphere in contact with the asperity and the second term describes the "noncontact" force between the large sphere and the flat surface separated by the asperity.

$$F_{ad} = \frac{A}{12z_o^2}\left[\frac{dD}{d+D} + \frac{D}{\left(1+\frac{d}{2z_o}\right)^2}\right] \quad (1)$$

Here A is the Hamaker Constant, z_o is the distance between two contact surfaces, and d and D are the diameters for the semispherical asperity and the large sphere, respectively. Other extensions of this work are similar [32,36,37], and are essentially single-asperity contact models, including the Rabinovitch model [38]. Interestingly, although Rabinovitch discussed that various scales of surface roughness and the frequency at which they are distributed may be of consequence, the main effect in their model was captured through the RMS of AFM-based roughness. Thus, in principle, the Rabinovitch model provides the same result as the Rumpf model with the asperity size d replaced by the RMS surface roughness. Rumpf model can be analyzed to gain insight into the role of the surface asperity size. An illustrative example depicting how each term in Eq. (1) is affected by asperity size, d, for a fixed size spherical fine particle, e.g., D of 10 μm, is presented in Fig. 2 through a log–log plot. The first term, shown as a green line, demonstrates that as the size of asperity increases, the separation between the pair of host particles increases hence the adhesion force reduces. However, the second term, shown as a red line, has an opposite trend and depicts the contact force between the asperity and contacting sphere, and it increases as a function of asperity size, d. The sum of these two terms, shown as a blue line, demonstrates why there exists an "optimal" asperity size for a given host particle size. Most interestingly, for fine powders of diameter D in the range 10–50 μm, the minimum value of the adhesion force occurs for asperity or guest particle size d of about 15–25 nm. Perhaps not coincidentally, some of the most used flow aids including fumed silicas as guest particles are in that size range and provide significant reduction and hence improved flowability after dry coating. In the absence of asperity, the adhesion force between two smooth spheres, shown as a black line in Fig. 2, is greater than that when the surface is *rough*. That points to an important fact that submicron-rough powders such as FCC particles [31] flow better than perfectly smooth spheres. That fact is evident as shown by a black marker on the blue line in Fig. 2, representing a 10 μm particle having a roughness of 200 nm diameter. To further illustrate the impact of the natural surface asperity sizes, two additional markers are plotted: a red marker depicting a rougher particle, e.g., having an asperity size of about 500 nm, and a green marker depicting a smoother (but not perfectly smooth) particle, e.g., having an asperity size of about 1 nm. This simple analysis demonstrates that the order of decreasing adhesion between a pair of particles, determined by particle roughness, is as follows: Perfectly smooth > nearly smooth (asperities ~ 1–2 nm), micro-rough (asperities ~ 500 nm), naturally rough (asperities ~ 200 nm), nano-silica coated (asperities ~ 10–30 nm).

Since the original Rumpf model provides significant insight through the asperity size analysis as shown in Fig. 2, one may question the need for extensions or new models. While it is true that most papers focus on digging deeper by including additional terms in the contact-model equations, they remain single asperity models that cannot identify the impact of the distribution of asperities along with the extent of guest particle surface area coverage (SAC). Since all natural surfaces have multiple asperities, single asperity models cannot include the impact of SAC and ensuing multiple contacts between the asperities and the contacting particle or surface. These deficiencies have motivated the development of multi-asperity models [33,43], including those that employ Fourier

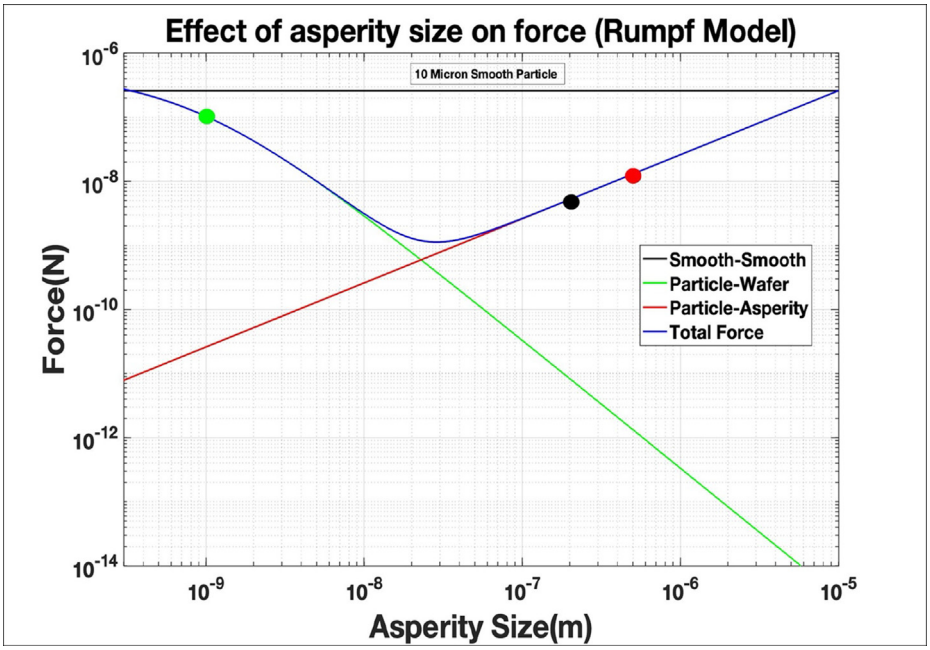

Fig. 2. Effect of asperity size on total force evaluated using Rumpf Model. A green marker denotes very smooth (not perfectly smooth) particle, a black marker denotes a particle having natural asperity of 200 nm diameter, and a red marker denotes a micro-rough particle having natural asperity of 500 nm diameter.

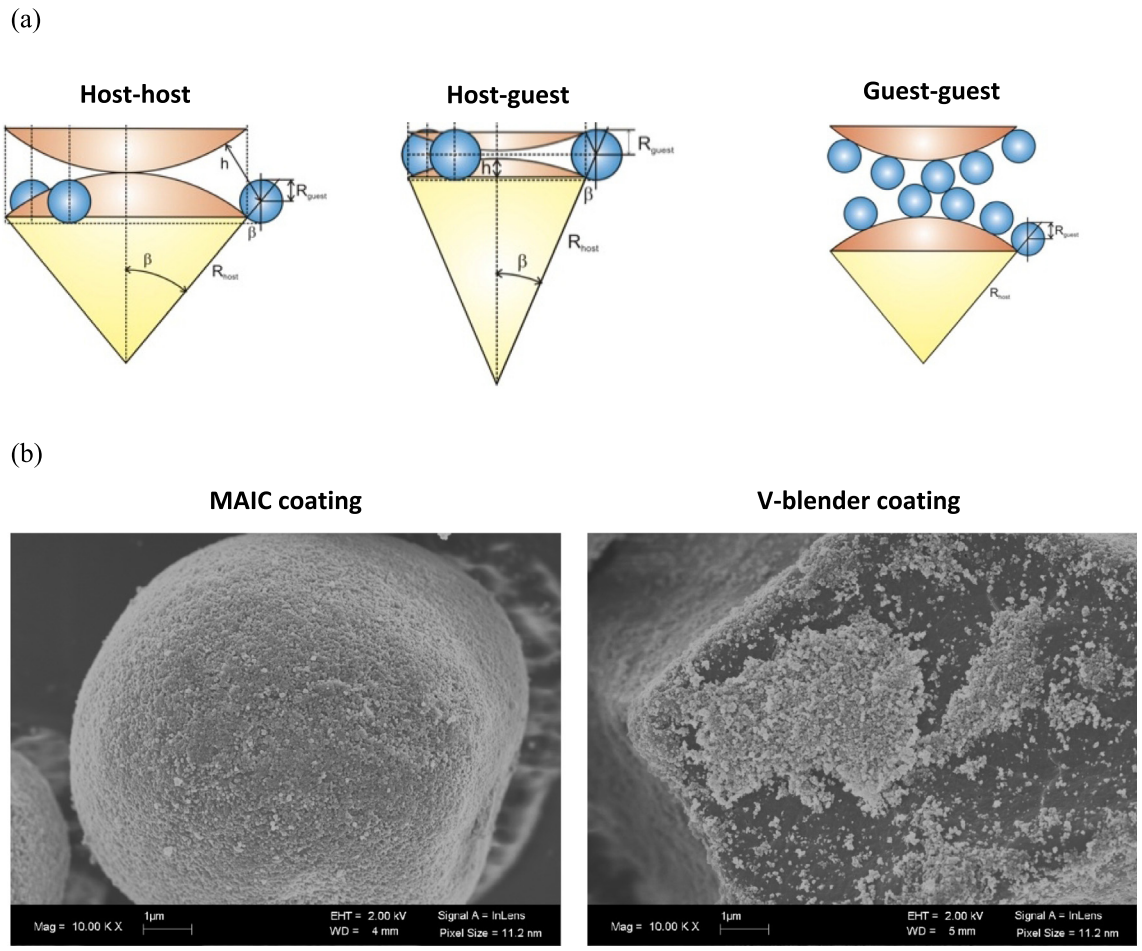

Fig. 3. (a) Schematic of three contact regimes defined in the Chen-NJCEP model; (b) Illustrative SEM images of the dry coating effectiveness for 1 wt% silica coating on cornstarch for high-intensity device (left-MAIC), and low-intensity device (right-V-blender).

transforms or fractals to simulate the host surface with hemispheres of varying sizes, placed at random locations to mimic the real surface [40,42,44,57]. Although the literature discusses a variety of simple to complex models, the most suitable model to date in terms of the predictive ability for understanding the impact of dry coating with guest particles is proposed by Chen et al. [33,43]. Chen model, hereafter called the *Chen-NJCEP model*, identifies three contact regimes; host–host, guest–host, and host–host, see Fig. 3a, and demonstrates that ideally, the coating coverage, defined in terms of the surface area coverage (SAC) should be about 30 % or higher for the dry coating to be most effective. In fact, that also explains that conventional low intensity mixing of guest particles does not produce satisfactory results because of the inadequate actual SAC, see Fig. 3b, the left image is for dry coating of silica in a high intensity mixer such as MAIC, and the right image is for using a low intensity mixer such as a V-blender. The model was derived under the assumptions of monodispersed, spherical host and guest particles and uniform, well-dispersed coating of guest particles [33]. The Chen-NJCEP model has three parts, see Eqs. (2), (3), and (5), respectively, for estimating the particle adhesion force, F_{ad}. Part 1 is for the host–host contacts, applicable when the amount of guest particles is very low and/or coating is ineffective. Part 2 is for the guest–host contacts when the amount of guest particles is sufficient to prevent the host–host contacts and it is naturally a function of SAC in percentage, valid for 0 < SAC < SAC_{crit}, the latter is the critical SAC for the value just above which the contact regime shifts to guest–guest. Theoretically, SAC_{crit} is about 30 % [33], hence above which, part 3 of the model is required, which is for the guest–guest contacts.

$$F_{ad} = \frac{A}{12}\frac{D}{2}\frac{1}{z_o^2} \tag{2}$$

$$F_{ad} = \frac{Ad}{4z_0^2} + \frac{A}{24\left(\sqrt{\left(1+\frac{d}{D}\right)^2 - \frac{1.21d^2}{SAC*D^2}} - 1\right)^2 * D} \tag{3}$$

$$SAC_{guest-host} = \frac{1.21}{1+2\left(\frac{D}{d}\right)} \times 100\% \tag{4}$$

$$F_{ad} = \frac{Ad}{8{z_0}^2} + \frac{AD}{24(2d+z_0)^2} \tag{5}$$

In the above equations, A is the Hamaker constant (material property, a function of surface energy), d is the particle size of the guest particle, z_0 is the minimum separation distance between two particles, the typical value being 0.4 nm [58,59], and D is the diameter of the host particle. The Hamaker constant could be calculated using Eq. (6), where D_0 is the cut-off distance (0.165 nm) and γ_d is the dispersive surface energy of the material, which could be measured through inverse gas chromatography (IGC) [60-62].

$$A = 24\pi {D_0}^2 \gamma_d \tag{6}$$

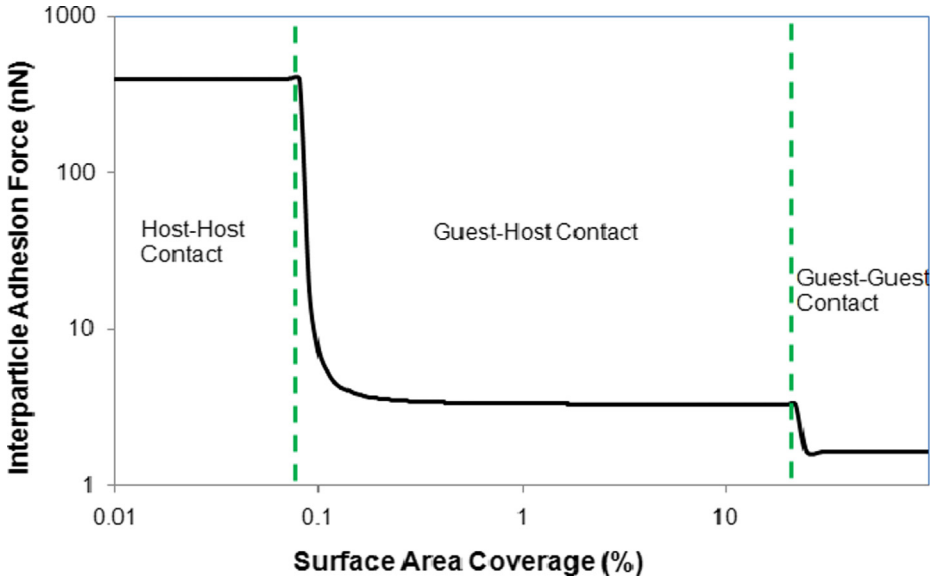

Fig. 4. Chen-NJCEP model, Eqs. (2)-(5), plotted for a host size of 15 mm, guest size of 20 nm, molecular separation distance of 0.4 nm, and Hamaker constant value of 10^{-19} J.

The Chen-NJCEP model is illustrated in Fig. 4, shown for a specific case of a host (~15 μm) and guest (20 nm), although the three-part behavior shown in the log–log plot would remain qualitatively similar for other relevant cases of host–guest pairs. The assumptions used for calculations in Eqs. 2–5 are: Monodisperse spherical host particles; monodisperse, non-agglomerated spherical guest particles; uniform coating of guest particles and no deformation of the guest or host particles; the Hamaker constant captures the effective surface energy at contact and, electrostatic and capillary forces maybe ignored for dry powders hence only van der Waals forces are applicable. Despite such limiting assumptions, this model has proved to be very applicable [14,21]. It is important to note that, Eq. (5) quantitatively differs from the Rumpf model, Eq. (1) and cannot be labelled as a "modified Rumpf model" as was done in [14,21]. That is because the Rumpf model implicitly assumes that the contact regime is guest–guest, yet it does not explicitly account for multiple guest particles from one particle simultaneously being in contact with a neighbor host particle. As a result, those contact forces are additive which could not be considered in Eq. (1).

Several important observations regarding the trend depicted in Fig. 4 may be made:

(1) Although only a little amount of nano-guest coating could lead to over an order of magnitude reduction in cohesion, theoretically as low as about 1 % SAC. However, in practice, higher SAC may be needed.
(2) Transition from host-host to guest–host or from host-guest to guest–guest contacts is rather sharp, although unlikely to be so sharp in real powder systems.
(3) The model can provide information about the cohesion reduction at particle scale, which could be up to two orders of magnitude. Therefore, the enhancement in bulk properties such as the flowability, powder bed unconfined yield strength (UYS), or bulk density are expected to be significant, but cannot be directly inferred.
(4) The trend shown is for idealized conditions where the dry coating is very uniform and guest particles are not agglomerated.

Regarding observations (1) and (2), it is important to note that the Chen-NJCEP model is deterministic and cannot provide statistically relevant information, which was more recently examined through Monte Carlo simulations [63]. However, regarding observation (3), referring to Fig. 5, angle of repose (AoR), unconfined yield strength (UYS), and bulk density of several industrially relevant powders as functions of SAC qualitatively follow the trend observed in Fig. 4, thus generally validating the veracity of the contact regime based, three-part Chen-NJCEP model. Regarding observation (4), the non-uniformity of coating may be tackled by either Monte Carlo type simulations [63] or through simulations such as those reported in [44,57]. It is expected that unless non-uniformity is extreme, which is unlikely because the dry coating is an event driven statistical process governed by the process intensity and time, normally occurring non-uniformity would not cause significant deviations in predicting cohesion reduction. In contrast, agglomeration of guest particles has double-negative effect; first, agglomeration leads to the effectively larger size of the guest, hence referring to Fig. 2, larger guest size means lesser cohesion reduction; second, guest agglomeration leads to reduced SAC, which also leads to lesser cohesion reduction. Since nano-sized guests tend to agglomerate as process intensity is increased [64-66], the effect needs to be quantified by developing a correction factor, which will be addressed in an upcoming paper.

2.2. Estimation of silica amount and type: Guest-host compatibility

Now that the importance of SAC is made evident by analyzing the Chen-NJCEP model, first order approximation of the amount of guest particles required can be obtained by assuming the projection of areas of all guest particles on the host particles using Eq. (7).

$$SAC = \frac{N \times \frac{\pi d^2}{4}}{4\pi\left(\frac{d+D}{d}\right)^2} \times 100\% \tag{7}$$

Correspondingly, Eq. (8) presents the required weight (wt%) of the guest particles.

$$\text{wt}\% = \frac{\left(Nd^3\rho_d\right)}{\left(D^3\rho_D\right) + \left(Nd^3\rho_d\right)} \times 100\% \tag{8}$$

The computed values of the wt% for a few selected examples of APIs and excipients from Table 1 are presented in Table 2 for 100 % SAC of R972P (hydrophobic) and A200 (hydrophilic) silicas. Since

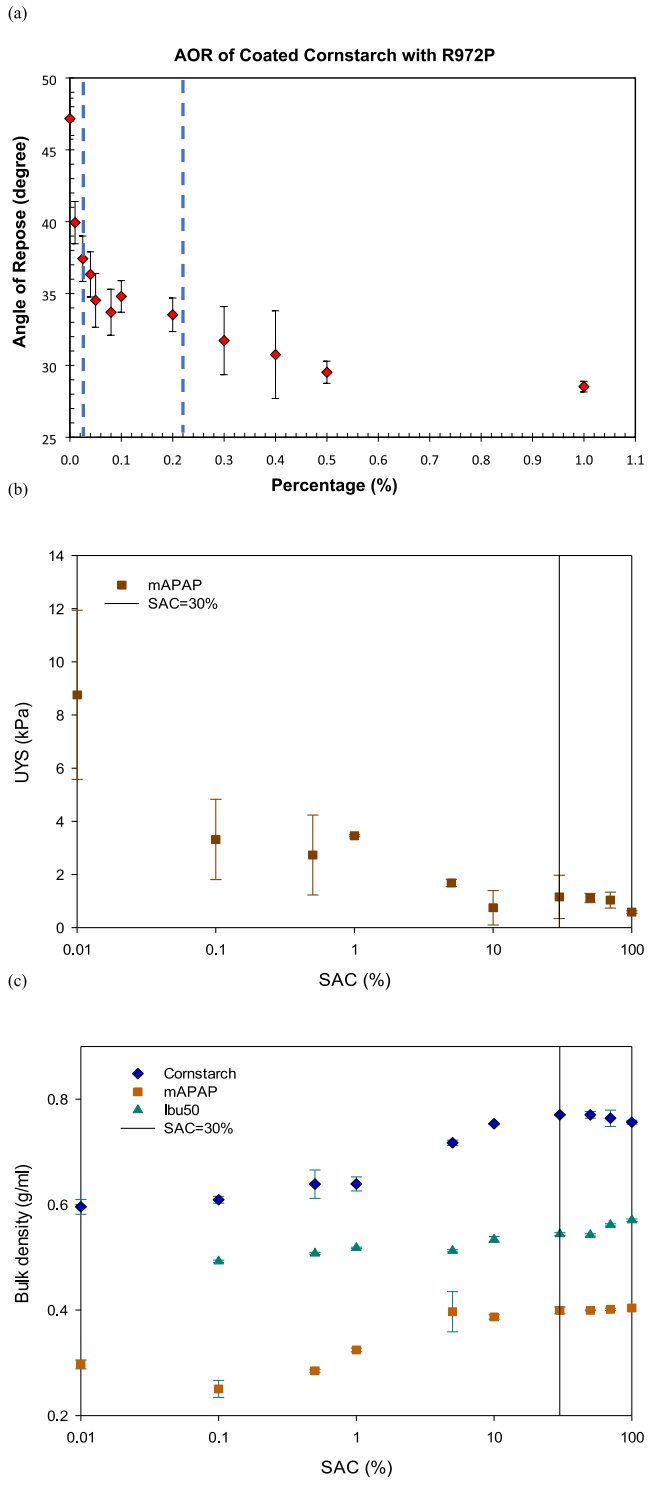

Fig. 5. (a) Angle of Repose (AoR) of cornstarch dry coated with silica R972P at different silica weight percentage, representing theoretical SAC. Two vertical lines separate host–host, host–guest, and guest–guest contact regimes. (b) Unconfined Yield Strength (UYS) of micronized acetaminophen (mAPAP) dry coated with silica R972P at different silica SAC. The vertical line represents SAC of 30 % and separates host–guest and guest–guest contact regimes. The trend of UYS and AoR is qualitatively like the model depicted in Fig. 4. (c) Bulk density (BD) of cornstarch, micronized acetaminophen (mAPAP), and Ibuprofen 50 dry coated with silica R972P at different silica SAC. The vertical line represents SAC of 30 % and separates host–guest and guest–guest contact regimes. The trend of BD is qualitatively like the model depicted in Fig. 4 for all three materials.

Table 2
Theoretical computation for guest material wt.% for 100% SAC of R972P (hydrophobic) and A200 (hydrophilic) silicas for a few selected cases of APIs and excipients of Table 1.

Material	R972P (wt%)	A200 (wt%)
micronized Acetaminophen (mAPAP)	3.32	1.86
Sorbolac 400 (Sorb400)	3.18	1.78
Pharmatose 450 (Pharm450)	1.76	0.98
Cornstarch (CS)	1.54	0.86
Pharmatose 350 (Pharm350)	1.42	0.79
Avicel 105 (Av105)	1.24	0.69
coarse Acetaminophen (cAPAP)	0.93	0.52
Ibuprofen 50 (Ibu50)	0.59	0.33
Avicel 101 (Av101)	0.32	0.18
Avicel 102 (Av102)	0.21	0.11
Theophylline (THPY)	0.2	0.11
Metformin (MTFN)	0.16	0.09
Avicel 200 (Av200)	0.14	0.07

A200 is finer than R972P, in all cases except two, the required amount is<1 wt%, and even smaller as the particle size of the host material increases. For R972P, being larger in size, the required wt% values are higher, hence for nearly half of the materials, over 1 wt% silica is required. As mentioned before, these equations assume uniform coating and no agglomeration of the guest particles. As the amount of silica increases, the deviation from these assumptions is likely to be higher, as predicted in [64] and quantified via image processing using software such as ImageJPro [33]. The reader is referred to Fig. 15 in [33], which demonstrated that as silica amount increased, deviation from theoretical SAC and actual SAC increased for silica coating on cornstarch, which is a very smooth, nearly spherical powder [33]. For materials unlike cornstarch, image processing to quantify silica SAC would pose additional challenges but would be worth the effort as silica amount is increased beyond 30 % SAC.

In terms of the host–guest compatibility, the model assumes that the flow aid can be uniformly coated. Therefore, a critical question is: how to know *a priori* which guest materials are compatible with the host material? There is little practical guidance on this topic although the concept of so-called cohesive-adhesive-balance (CAB) has been proposed in the inhalation literature. Unfortunately, that requires measurement of adhesive forces between guests as well as guest and host using an AFM, which is not practical when the guests are nano-sized. In our group, the interactive mixture model [67] is used through the spreading coefficient of material 2 (Guest) over material 1 (Host), $\lambda^{2/1}$, and vice versa.

$$\lambda^{2/1} = 4\left[\frac{\gamma_1^d * \gamma_2^d}{\gamma_1^d + \gamma_2^d} + \frac{\gamma_1^p * \gamma_2^p}{\gamma_1^p + \gamma_2^p} - \frac{\gamma_2}{2}\right] \tag{9}$$

Here γ_1 and γ_2 are the surface energies of materials 1 and 2, respectively, and the superscripts d and p are the dispersive and acid-base (otherwise referred to as polar) components, respectively. Using the spreading coefficient, the guest–host suitability may be determined based on the absolute difference between $\lambda^{2/1}$ and $\lambda^{1/2}$. It is proposed that if the difference is large, the guest is likely to coat and if it is small, it is unlikely to coat. Our preliminary recommendation assumes that the particle 2 is smaller than 1, which would be an obvious case for dry coating. Such prediction was found to work well in the coating of hydrophilic versus hydrophobic silica onto different API and excipient powders; see Table 3. Selected examples of these are also shown in Fig. 6. While these examples indicate that

Table 3
Suitability of the guest material and dry coating based on the surface energy measurements. The difference in the spreading coefficient determines suitability; best when it is > 10, poor, when it is < 5, and acceptable in between.

Host	LW dispersive surface energy γ_d (mJ/m^2)	Lewis Acid-Base surface energy γ_p (mJ/m^2)	Difference in spreading coefficient (host–guest)	
			M5P	R972P
MAPAP	46.38	5.05	**6.78**	**22.59**
CAPAP	40.86	4.19	**5.97**	**10.51**
IB90	48.33	4.78	**10.14**	**25.95**
IB50	38.92	4.27	**9.69**	**6.79**
AV101	42.33	4.93	**1.56**	**14.26**
AV102	56.05	8.97	**33.97**	**50.44**
AV105	47.80	6.50	**12.52**	**28.34**
Guest Materials				
M5P	44.68	3.36		
R972P	34	5.75		

the spreading coefficient may be adequate to determine the host and guest compatibility, there are situations where the processing conditions may have an impact, see for example, cases where the coating was better than predicted using this approach [68]. Such positive deviations from the predictions are likely because the dry coating devices are high-intensity devices whereas the prediction based on surface energy does not account for the dynamics of process intensity and is applicable only for low-intensity mixing.

2.3. Estimation of nondimensional cohesion via the granular Bond number

As mentioned earlier, it is useful to consider the Bond number, Bo_g, to better understand the relative cohesion. For dry, uncharged powders, it is essentially the ratio of particle–particle van der Waals (vdW) force to particle weight. Thus, the Bond number for dry powders maybe defined as in Eq. (10).

$$Bo_g = \frac{F_{vdW}}{W_g} \tag{10}$$

Here F_{vdW} is the interparticle cohesive force, and W_g is the particle weight. The calculation of particle weight (W_g) is straightforward, see Eq. (11), where D is the median particle size and ρ_p is the particle (true) density of the powder. The acceleration due to gravity (g) is approximated to be 9.8 m/s^2.

$$W_g = \frac{\pi}{6} D^3 \rho_p g \tag{11}$$

As mentioned before, the asperity size (d) maybe approximated to be 200 nm for all powders, based on experimental work by Massimalla and Donsi [31]. However, as was discussed recently [68], the assumption of the natural asperity size of 200 nm diameter is not valid for many particles and may require extensive analysis or a rough estimate obtained from SEM images. In addition, as was discussed in our recent paper [68], applying an empirical equation [28] as a function of the host particle size may be equally erroneous. Hence, this is an area that requires further investigation because accurate estimation of surface roughness is non-trivial

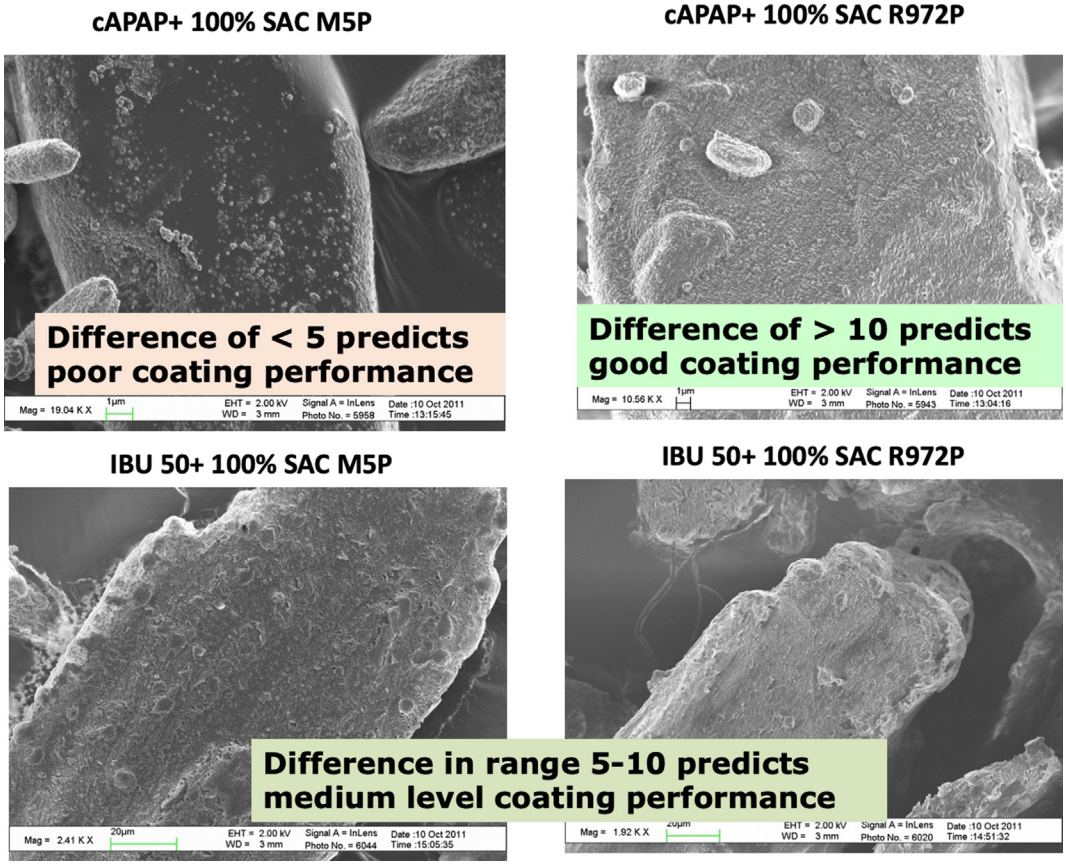

Fig. 6. SEM images of exemplary cases of dry coated APIs with silica using LabRAM. (top) The spreading coefficient based prediction for coarse acetamenophen (~30 mm) coating was: poor for hydrophilic (M5P – left) silica and good for hydrophobic (R972 – right) silica. (below) The spreading coefficient based prediction for ibuprofen (~50 mm) coating was: better for hydrophilic (M5P – left) silica than for hydrophobic (R972 – right) silica.

Table 4
Granular Bond numbers calculated using the Chen-NJCEP model before and after dry coating for the cases of APIs and excipients of Table 3.

Material	Bo_g (uncoated)	Bo_g (After coating with R972P 100% SAC)	Bo_g (After coating with A200 100% SAC)
micronized Acetaminophen (mAPAP)	20,069	1587	1151
Sorbolac 400 (Sorb400)	22,626	1909	1380
Pharmatose 450 (Pharm450)	369	30.9	23.9
Cornstarch (CS)	415	47.8	36.6
Pharmatose 350 (Pharm350)	97	8.76	7.08
Avicel 105 (Av105)	1505	117	87.4
coarse Acetaminophen (cAPAP)	368	33.6	26.1
Ibuprofen 50 (Ibu50)	65	6.4	5.32
Avicel 101 (Av101)	21.4	1.97	1.71
Avicel 102 (Av102)	7.8	0.56	0.53
Theophylline (THPY)	4.7	0.42	0.41
Metformin (MTFN)	2.3	0.22	0.23
Avicel 200 (Av200)	1.86	0.17	0.18

since even the use of AFM leads to asperity size to be a strong function of the area of scrutiny. Regardless, as was conveyed in [68], SEM based estimation may be reasonable in some of the cases and then Chen-NJCEP model would be applicable under the assumption that only asperity-host or asperity-asperity contacts are possible. Better means to estimate the size and distribution of asperities, including SAC %, are the topics of interest and would be addressed in a forthcoming paper. In contrast to as received or uncoated powders, in cases where dry coating with nano-silica guest particles is performed, the size of silica is the right choice for the value of d, and then Chen-NJCEP model would apply along with the SAC % corresponding to guest wt%.

In summary, the Bond number of a powder may be estimated using the equations discussed above along with a few particle-scale inputs; characteristic particle size, usually Sauter mean diameter ($D_{3,2}$), particle (true) density (ρ_p), asperity size (d) along with its SAC %, and dispersive surface energy (γ_d). As discussed above, there are challenges associated with some of these measures, e.g., the asperity size and actual SAC %. Nonetheless, with reasonable estimates for those, the Chen-NJCEP model could be used for estimation of the Bond number, and consequently, quantification of bulk-scale behavior using these particle-scale measurements. As illustrative examples, Bond numbers before and after dry coating with either of two different types of silica are computed and provided in Table 4 for the materials listed in Table 2. A quick examination reveals that dry coating leads to at least an order of magnitude reduction in the Bond numbers for nearly all the cases, which is mostly in line with the expected cohesion reduction illustrated in Fig. 4. It is useful to note that whereas the model predicts cohesion reduction of about 2 orders of magnitude for finer powders, that is only valid for very smooth, spherical powders. For the type of powders listed in this table, they may have rougher surfaces and as seen in Fig. 2, the cohesion reduction for those could be about one order of magnitude, i.e., for powders that mimic those schematically depicted by red or blue markers in Fig. 2. To close this section, the power of the Bond number as a scaling parameter for bulk properties such as the bulk density is illustrated in Fig. 7, adapted from [21]. This milestone works greatly extended previous examples of the power-law relationship between the Bond number of bulk properties [24,33]. In Fig. 7(a), porosity, as a dimensionless measure of the packing density of six API powders and four excipient powders are plotted as a function of particle size before and after dry coating with one of six different guest powders. There is significant scatter for the dry coated powders, which is natural because, for the same particle size, the packing density of dry coated powders greatly increases as the guest particle size decreases. For all these cases, the Bond number works very well as a dimensionless scaling parameter, see Fig. 7(b). Most of the scatter seen in Fig. 7(a) is eliminated, indicating the suitability of the Bond number as a scaling parameter to link particle-scale properties with bulk-scale properties of powders. Although outside the

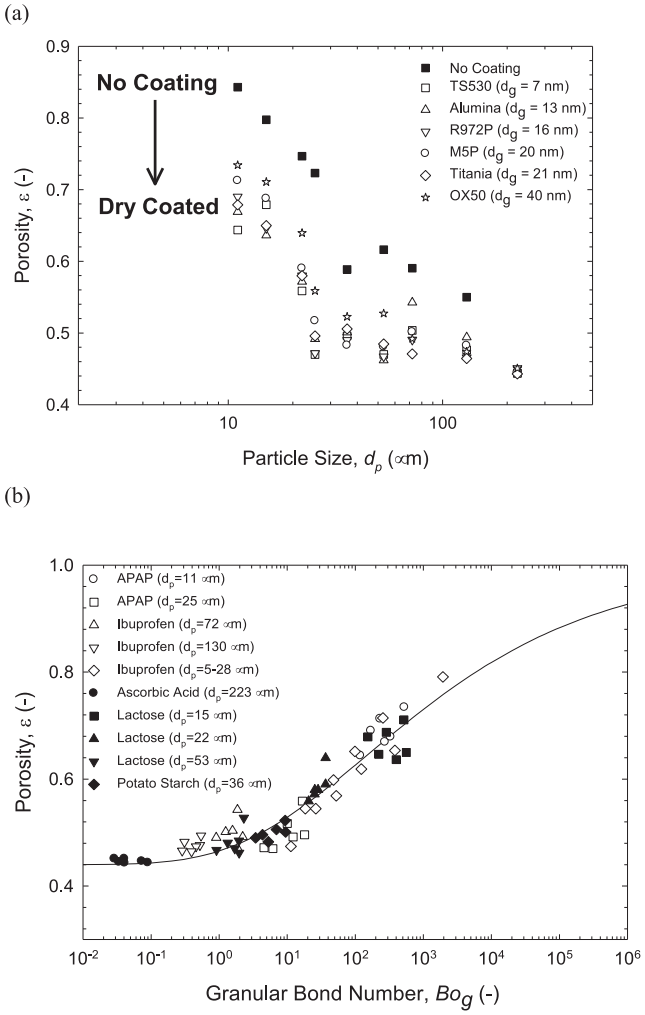

Fig. 7. Linking particle and bulk scales. (a): Particle size vs. porosity of powders. (b) Bond number vs. porosity of packed powders, demonstrating significantly reduced scatter.

scope of this paper, the topics of incorporating the effect of the full PSD of the powder sample instead of just a single illustrative size such as d_{50} or $d_{3,2}$, and mixing rules for blend bulk property prediction are important ones for utilizing the Bond number as a basis for better predicting powder or blend bulk properties.

2.4. Bulk powder flowability assessments

Assessment of powder flowability serves a critical role in process operation and design. Consequently, accurate and precise measurements and classification a pivotal step in powder characterization. Bulk powder flowability can be assessed using either the shear testing, Carr index, Hauser ratio, the angle of repose (AoR), or an orifice meter. As outlined by Thalberg et al [19], different measures have different discernibility in different flow regimes. For example, the AoR is most discernible for well flowing powders and so is the orifice meter. In contrast, the FFC as an outcome of shear testing has better discernibility for cohesive powders. Since the emphasis here is on cohesive powders and their flow enhancements, shear testing, an important and well accepted powder characterization method, was selected as the characteristic flow assessment method. Shear testing is based on the rheological and shear properties of a powder, resulting in the flow function coefficient, *FFC,* as the *ratio* of the major principal stress(σ_1) to the unconfined yield strength (σ_c). Its importance and assessment have been outlined in classic theory of incipient plastic flow developed by Dr. Jenike in his doctoral thesis [69]. Additional details of this topic may be also found in [70,71]. The Freeman FT4 powder rheometer with shear cell module (Freeman Technology Ltd., Worcestershire, UK) was used and 3 kPa pre-consolidation stress was chosen based on consolidation stresses normally encountered by pharmaceutical powders for a 25 mm diameter glass vessel of 10 ml volume (25 mm × 10 ml split vessel). Further details of the use of FT4 for obtaining FFC values can be found elsewhere [2,8,61,72]. The flow function coefficient FCC (defined as the ratio of consolidation stress to the unconfined yield stress), and cohesion coefficient (shear strength at zero normal stress) were obtained. The data in Table 1 includes a variety of APIs and excipients ranging in median particle size, d_{50}, from about 4.2 to 225 μm [10,12,14,34,52,53,62,68].

3. Experimental

3.1. Dry coating devices and LabRAM as a material sparing benchmarking device

The dry coating may be performed using high intensity mixing devices, for example, traditional dry coating devices such as the Hybridizer and Mechanofusion [73–80], as well as the magnetically assisted impaction coater (MAIC) [4,5,81]. Since these are batch devices and may not be easily amenable to routine use and cost-effective scale-up in industry, our group has developed the use of other devices, including two continuous devices, and one batch-mode benchmarking device. The Fluid Energy Mill (FEM) is a continuous device that has been developed as a simultaneous milling and dry coating device in a two-step process, the first step being pre-blending of host and guest before the second step of milling and coating [1]. A conical mill or a comil is another continuously operated device that has been used for dry coating cohesive powders [2,82,83]. More recent papers have examined multiple APIs and excipients and demonstrated that when properly used, comil can achieve a good coating of either hydrophilic or hydrophobic silica for all these materials, leading to significant property enhancements [8,13]. The FEM device is most suitable for finer powders and those that are normally obtained by milling so that the milling step could be preceded by pre-blending with the guest material. The comil device is generally suitable for powders that are not too fine, i.e., < 10 μm. These two devices are easily available in the industry and have a great promise for commercial usage. However, neither of them is suitable as a material sparing device, nor very convenient for preformulation assessment of the impact of dry coating on flow and other property enhancements. Therefore, having a reliable material sparing device for benchmarking purposes is highly desirable. Towards that objective, our group has utilized the MAIC device in past as a proof-of-concept material-sparing device [4,5]. In addition, MAIC operating parameters have been investigated to ascertain effective coating and avoiding attrition [4], and it has been also used as a benchmarking device against the comil [8]. However, the broader adoption of MAIC as an industry relevant device has been handicapped by the fact that the MAIC device uses magnetic particles that come in direct contact with the powder sample, leading to the possibility of contamination. Motivated in part by such concerns, our group has investigated the use of a relatively new, laboratory scale high-intensity vibratory device, called LabRAM, which is very effective in achieving uniform discrete nanoparticle coating. Major advantages of LabRAM include, no internal moving parts, the powder containing vessel can be made of pharmaceutically acceptable materials such as stainless steel, it is less prone to powder attrition despite use of up to 100 g force, and importantly, it may be used as a material sparing device at lab-scale. Therefore, it has been used as a material sparing device to dry coat a variety of pharmaceutical drug and excipient powders [7,9,10,12,14,21,34,52,62,68,84]. Here, a limited investigation of the selection of typical operating parameters for LabRAM is presented like what has been presented before for MAIC [4] and Comil [8]. The results for flowability (FFC) of selected APIs after dry coating are presented along with comparative results of the MAIC outcomes.

The analysis of variance (ANOVA) and main effects plot drawn using Minitab, not shown for the sake of brevity, considered the effect of all the factors in a 2^5-factorial design of LabRAM experiments; mixing time, intensity, fill level, the guest type, and host API type on the bulk density. Conditioned bulk density being a key indicator of all flow related property enhancements, was selected as the response factor [2,4,6,82]. It was concluded that the maximum bulk density was attained at 70% intensity, 5 min processing time, and 75% fill level. These conditions were used to dry coat five APIs; micronized APAP (A1), coarse APAP (A2), ibuprofen 90 (A3), ibuprofen 50 (A4), ascorbic Acid (A5), and six excipients, Avicel 101 (E1), Avicel 102 (E2), Avicel 105 (E3), Pharmatose 350 (E4), Pharmatose 450 (E5), Pharmatose DCL11 (E6), with either silica R972P or M5P, or magnesium stearate (MgSt) as a typical lubricant. Particle size measurements before and after dry coating for all these cases were carried out and indicated that at the selected conditions, LabRAM did not lead to appreciable attrition; see Fig. 8. Bulk property enhancements after dry coating at those selected conditions for all five APIs and six excipients are illustrated in Fig. 9 for conditioned bulk density (BD) as an exemplary property. Considering that BD of greater than about 0.38 g/ml is good and may promote direct compaction, dry coating led to that level (or well exceeded) in all cases including for five materials that are very fine (<30 μm). These results also indicate that LabRAM processing enables significant BD enhancements for all cases amounting to an increase of 20–100 %, except for ascorbic acid which has very high BD to begin with. The performance of LabRAM in terms of flowability enhancement (FFC) for the APIs that typically have poor flowability is compared with MAIC for dry coating of R972P at 100% SAC in Fig. 10. As shown, the LabRAM coating led to flowability enhancement by one or multiple regimes (defined before [18]), generally outperforming MAIC.

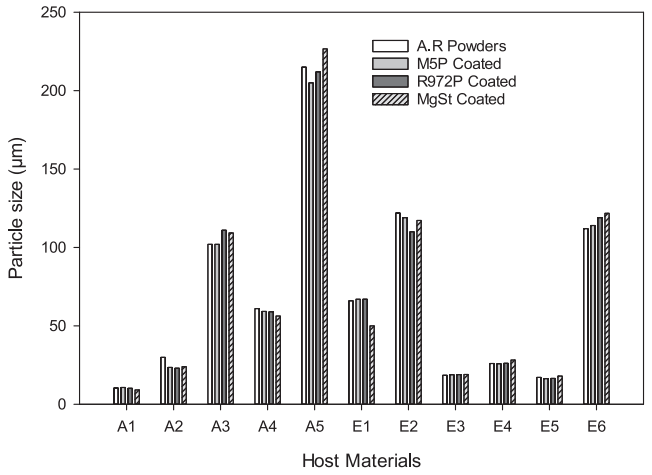

Fig. 8. Particle size (d_{50}) of uncoated and dry coated (with M5P, R972P or MgSt) APIs (micronized APAP, coarse APAP, ibuprofen 90, ibuprofen 50, ascorbic Acid) and excipients (Avicel 102, Avicel 105, Pharmatose 350, Pharmatose 450, Pharmatose DCL11).

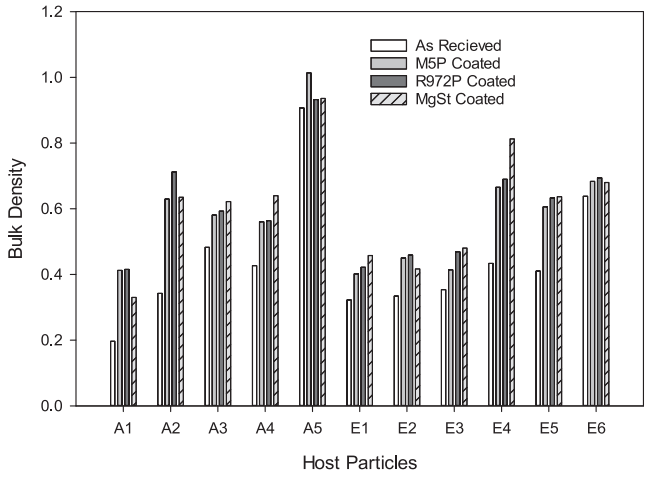

Fig. 9. Bulk Density (g/mL) of uncoated and dry coated (with M5P, R972P or MgSt) APIs (micronized APAP, coarse APAP, ibuprofen 90, ibuprofen 50, ascorbic Acid) and excipients (Avicel 102, Avicel 105, Pharmatose 350, Pharmatose 450, Pharmatose DCL11).

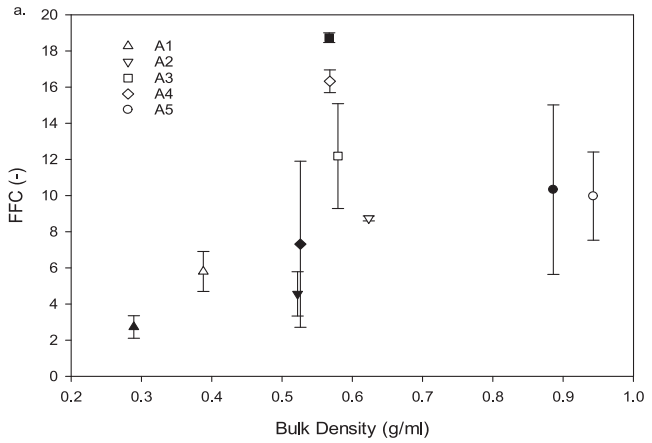

Fig. 10. Comparison of flowability (FFC) enhancements with LabRAM (open markers) versus MAIC (filled markers) for 100% SAC R972P coated micronized APAP (A1), coarse APAP (A2), ibuprofen 90 (A3), ibuprofen 50 (A4), and ascorbic Acid (A5). For reference, FFC values for uncoated APIS are 1.2, 2.7, 4.7, 4.2, and 5.7, respectively.

3.2. LabRAM-based dry coating for mitigating flow, packing, agglomeration, and dissolution problems with pharmaceutical powders

Dry coating using different devices has been shown to reduce the cohesion of fine powders, leading to improved bulk powder properties, e.g., the flowability, packing density, agglomeration, fluidization, and dissolution [4,8,17,32-34,85-88]. In this paper, first, the flowability enhancements for the powders listed in Table 1 after LabRAM-based dry coating with A200 (100 % SAC) are plotted in Fig. 11(a) as a function of Sauter mean diameter. For the sake of comparison, uncoated FFC values are also included. This plot indicates that particle size alone cannot capture the effect of coating, as was the case for the porosity trends shown in Fig. 7(a). These results are also provided in Table 5 for an easy depiction of the extent of flow regime enhancements for each powder. A graphical view of the number of flow regimes shifted upwards as a function of the starting regime is presented in Fig. 11(b). While there is significant scatter, the trend line indicates that for a powder in the *very cohesive* regime, dry coating leads to an upward shift by an average of over two flow regimes, i.e., moving to *easy flow* regime. Likewise, from cohesive regime, the upward shift is by one or two regimes, hence moving to *easy flow* or *free flowing* regime. For example, of 8 *very cohesive* powders, flowability was enhanced by one regime for 2, two regimes for 5, and three regimes for 1. Understandably, if the starting regime is *easy flow* or *free flowing*, the flow regime upward shift is naturally limited. The main message is that for the powders that need flow enhancements, i.e., those in the *very cohesive* or *cohesive* regimes, the dry coating could push them upwards by one to three regimes. For the poor flowing powders that could not achieve such enhancements after dry coating, further research is required to identify which features may cause dry coating effectiveness to be poor. Some of the potential causes be their surface morphology including the scale of roughness, deviation from spherical shape, high aspect ratios or specific surface area (SSA) being larger than that of an equivalent spherical particle of the same size. Dry coating of such powders may require further refinement of formulations and conditions including the type and amount of silica, as well as process intensity and time.

In addition to enhancements in flow and packing density after dry coating, reduced cohesion is expected to decrease fine powder agglomeration, as may be expected based on the significant reduction in the Bond number [29]. That has indeed been the case for fine pharmaceutical powders as has been reported in recent papers [34,62,68]. It has been shown that dry coating can reduce the agglomeration ratio (AR), defined as the size of an agglomerate normalized by the primary particle size, by an order of magnitude [68]. Three different milled ibuprofen powders, Ibu5, Ibu10, and Ibu20, see Table 1, were dry coated with 100 % SAC of either hydrophilic silica A200 or hydrophobic silica R972P and their flowability (FFC), bulk density (BD), and agglomeration were measured [68]. Most interestingly, as it has been recently reported, fine powder agglomeration before and after dry coating could provide a quick screening indication of its effectiveness in cohesion reduction, hence FFC and BD enhancements; see FFC – AR and BD – AR relationships in Fig. 12(a) and 12(b). After dry coating, AR values were reduced by an order magnitude for all three milled API powders, which lead to one or two flowability regime enhancements and an almost doubling of the BD values. For these powders, it is evident that for AR < 5, achieved simply by dry coating, both flowability and bulk density are greatly increased making them well flowing and well packing powders.

The impact of reduced cohesion, hence reduced agglomeration, has another major impact, namely improved dissolution rate from fine, poorly water-soluble APIs such as milled ibuprofen powders. As particle size decreases, the dissolution rate is expected to get

(a)

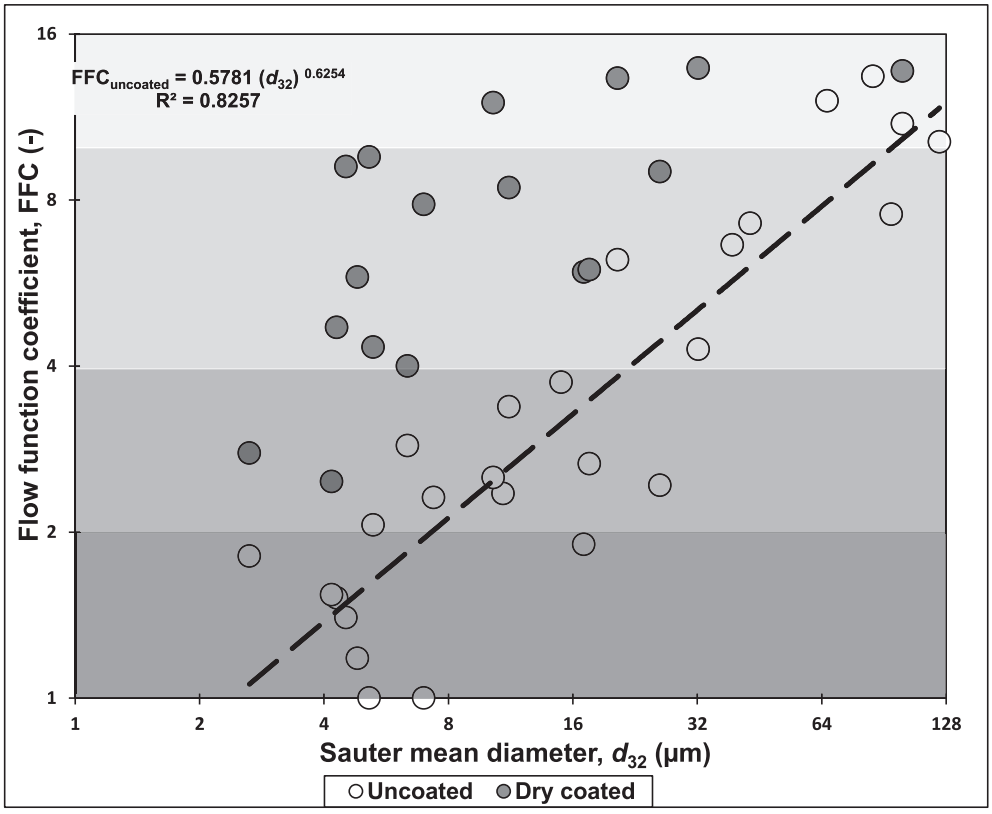

(b)

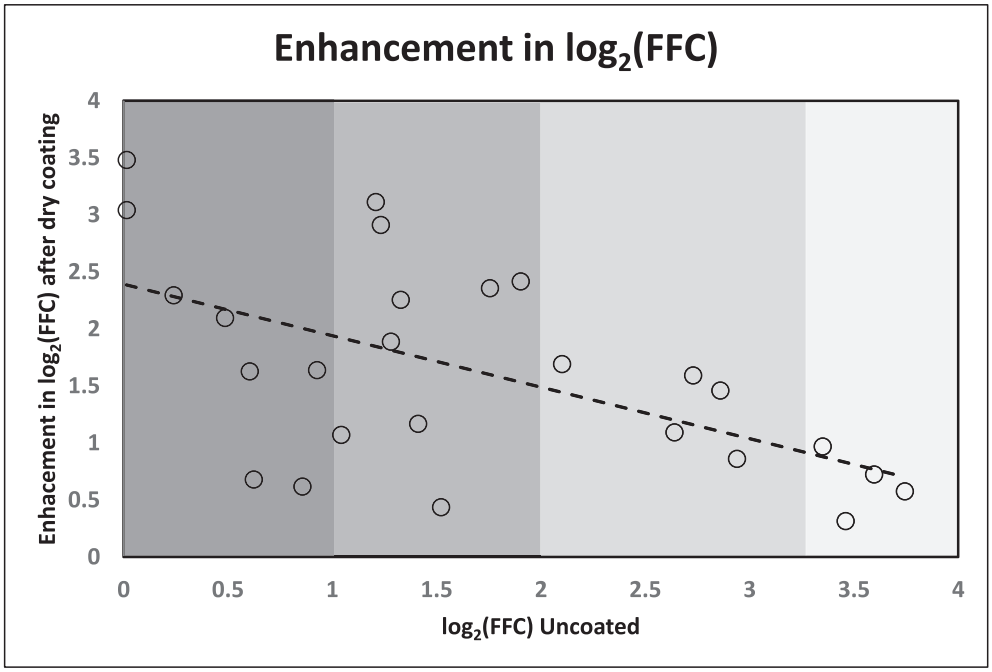

Fig. 11. (a) Flowability (FFC) of 26 pharmaceutical powder materials of Table 1, plotted as a function of Sauter mean diameter, in log–log (base 2) plot before and after the dry coating. A power law trend line fitted for the uncoated powder appears to capture the trend. However, the scatter for the dry coated powders is excessive, naturally due to notable FFC improvement. (b) The enhancements in FFC (log basis 2) after dry coating are shown as a function of the FFC (log basis 2) of the uncoated. The fitted line indicates the general trend.

Table 5
The API and excipients powders from Table 1, where the FFC after dry coating with 100 % SAC coating of A200 and resulting flow regime and the level of regime enhancements are shown.

Materials	FFC	Flow Regime Before Coating	FFC After Coating (A200 100% SAC)	Flow Regime After Coating (A200 100% SAC)	Regime Improvements
Inhalac500	1.8	Very cohesive	2.8	Cohesive	1
Inhalac400	1.5		2.5		1
Sorbolac 400 (Sorb400)	1.5		4.7	Easy Flowing	2
Fenofibrate (FNB)	1.4		5.9		2
micronized Acetaminophen (mAPAP)	1.2		5.8		2
Ibuprofen milled to 5 microns (Ibu5)	1		8.3		2
Ibuprofen milled to 10 microns (Ibu10)	1		11.3	Free Flowing	3
Pharmatose 450 (Pharm450)	1.9		5.9	Easy Flowing	2
Itraconazole (ITZ)	2.1	Cohesive	4.33		1
Griseofulvin (GF)	2.9		3.9	Cohesive	0
Granulac 230 (Gran230)	2.3		20	Free Flowing	2
Granulac 200 (Gran200)	2.5		12		2
Avicel 105 (Av105)	2.4		17.7		2
Ibuprofen milled to 20 microns (Ibu20)	3.4		17.3		2
Cornstarch (CS)	3.7		20		2
coarse Acetaminophen (cAPAP)	2.7		5.9	Easy Flowing	1
Pharmatose 350 (Pharm350)	2.4		9		1
Ibuprofen 70 (IBU70)	6.2	Easy Flowing	13.3	Free Flowing	1
Ibuprofen 50 (Ibu50)	7.4		13.8		1
Lactose 120 (Lac120)	4.3		20		1
Avicel 101 (Av101)	6.6		20		1
Theophylline (THPY)	7.4		13.9		1
Avicel 102 (Av102)	7.7		20		1
Pharmatose DCL11 (DCL11)	7.5		20		1
Avicel 200 (Av200)	12.1	Free Flowing	13.7		0
Ascorbic Acid (AA)	13.4		20		0

faster as per the Noyes-Whitney equation [89]. Unfortunately, as has been shown before, milling leads to powder agglomeration which negates the expected advantage of reduced particle size [34,90]. Such a trend is evident in Fig. 13, which demonstrates that dissolution rate gets slower as particle size gets finer, see solid curves for milled powders without coating. In contrast, dry coating led to not only faster dissolution, but making the dissolution rate to be in line with the Noyes-Whitney equation, see dashed curves in Fig. 13. Most surprisingly, the results plotted in Fig. 13 are for dry coating with hydrophobic silica, which is counterintuitive since the hydrophobic coating is expected to slow the dissolution rate due to reduced wettability. The reason for the opposite behavior is due to greatly reduced agglomeration even when the surface hydrophobicity increases after coating with R972P [34].

Overall, dry coating has been shown to enhance powder bulk properties such that typical fine powder of 10 μm size flows, packs, and fluidized like a 100 μm powder, and its agglomeration is reduced by an order of magnitude, so much so that even after hydrophobic coating, it could promote faster dissolution. In the next section, the positive impacts of dry coating of a single component of blends are highlighted through a few selected examples.

3.3. Enhancement of blend properties for enabling direct compression tableting: Mixing synergy due to one dry coated component

Several previous papers examined the influence of dry coated fine API in a multi-component blend to potentially enable direct compression (DC) tableting at higher drug loadings. The first paper examining such a topic considered micronized ibuprofen (~20 μm) at 30, 50, or 70 % drug loading in a formulation also containing Crospovidone (5 wt%), MgSt (1 wt%), hydrophilic silica M5P (1 wt % of the API), and the remainder being equal parts of Avicel pH 102 and Pharmatose DCL 11 [6]. In Fig. 14(a), the main outcomes are shown in a two-dimensional *processability phase map* of FFC versus BD for three uncoated API and coated API blends [6]. The shaded rectangular region indicates the possibility of DC tabletability based on industry guidelines and typical flow and bulk density properties of Avicel PH-102, i.e., FFC of about 6.8 and BD of about 0.38 g/ml [91]. Remarkably, dry coating of fine API led to DC possibility for all three drug loadings [6]. In addition, it was shown in that paper that dry coating also led to a greatly improved API dissolution rate without any loss of tabletability [6]. Enabling DC processability for higher drug loading formulations by dry coating an API was further put to a stress-test by

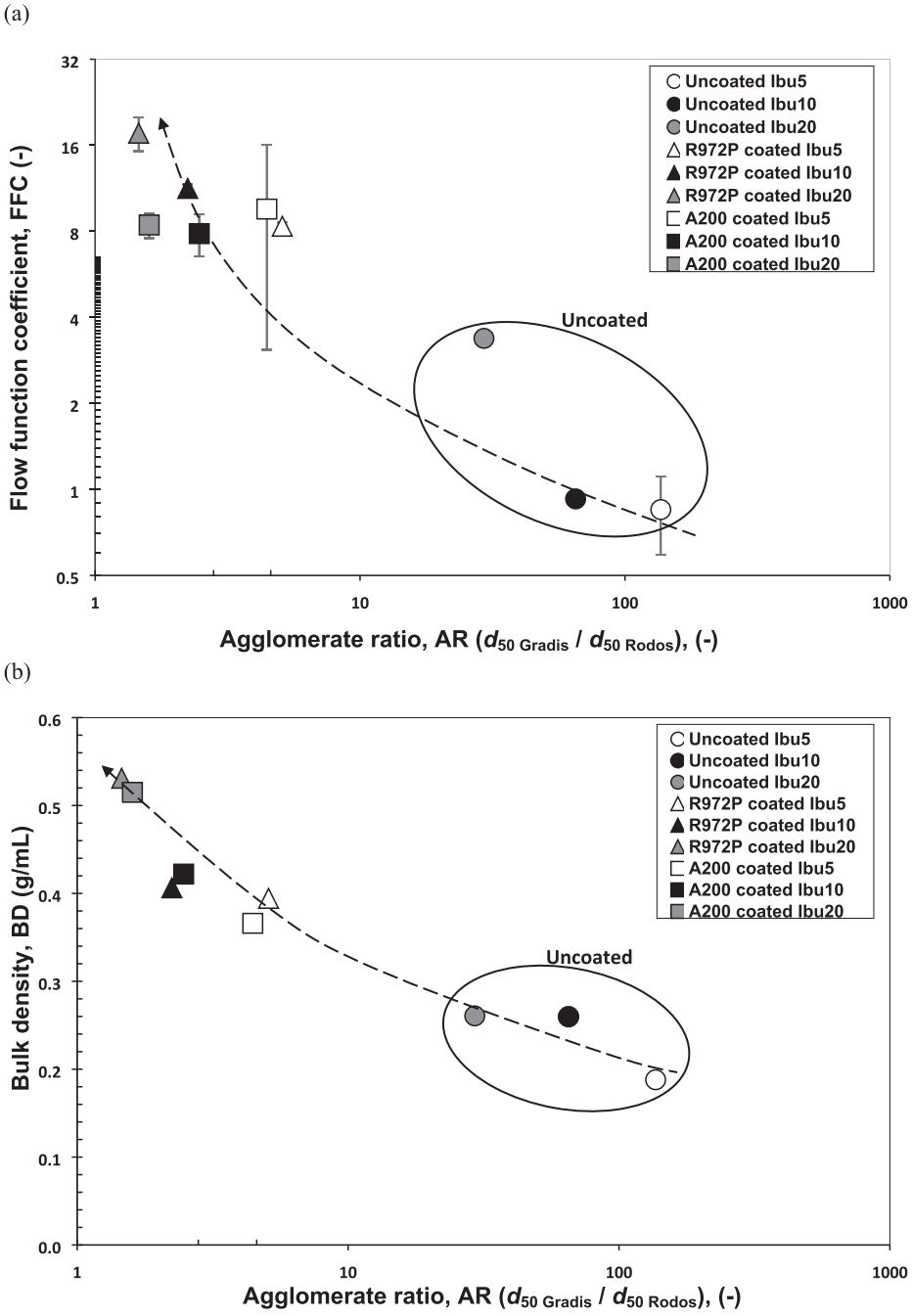

Fig. 12. The relationship between the agglomerate ratio (AR) and bulk properties of three fine APIs (Ibu20, Ibu10, Ibu5). (a) FFC as a function of AR. (b) BD as a function of AR. The dotted lines are for illustrating the trends.

considering finer, more flow-challenged mAPAP (~10 μm) [7]. In that groundbreaking work, not only the potential for DC processibility of mAPAP was demonstrated at 60 % drug loading, but it was also shown that with mAPAP being dry coated, the size of the excipients did not have a major influence and there was no loss of tabletability. That work considered coarse excipient formulation using Avicel pH 102 and Pharmatose DCL 11 and fine excipient formulation using Avicel pH 105 and Pharmatose 450, and demonstrated that dry coated mAPAP led to nearly the same values of BD and FFC, both being in the DC regime, see Fig. 5 in that paper [7]. Such outcomes were further verified and generalized with either hydrophilic (M5P) or hydrophobic (R972P) silicas and three different APIs, mAPAP, IBU20, and cAPAP each at 60 % drug loading [52]. It was shown that for all three APIs, with either silica coating, the finer excipient formulation reached DC processability as their FFC and BD exceeded 6.8 and of 0.38 g/ml, respectively. Interestingly, for dry coated cAPAP, the coarsest of the three APIs, DC processability was also attained for coarser excipient formulations.

The results for enhanced DC processability of high drug loaded formulations by the dry coating of finer APIs, which have intrinsically poor flowability, are intriguing in several ways. First, dry coating, which reduces powder surface energy, did not lead to the anticipated loss of tabletability. Second, finer excipient-based formulations fared as well as or better than coarser excipient-based formulations; another counter-intuitive outcome considering that placebo blends of finer excipients have poor flowability and bulk

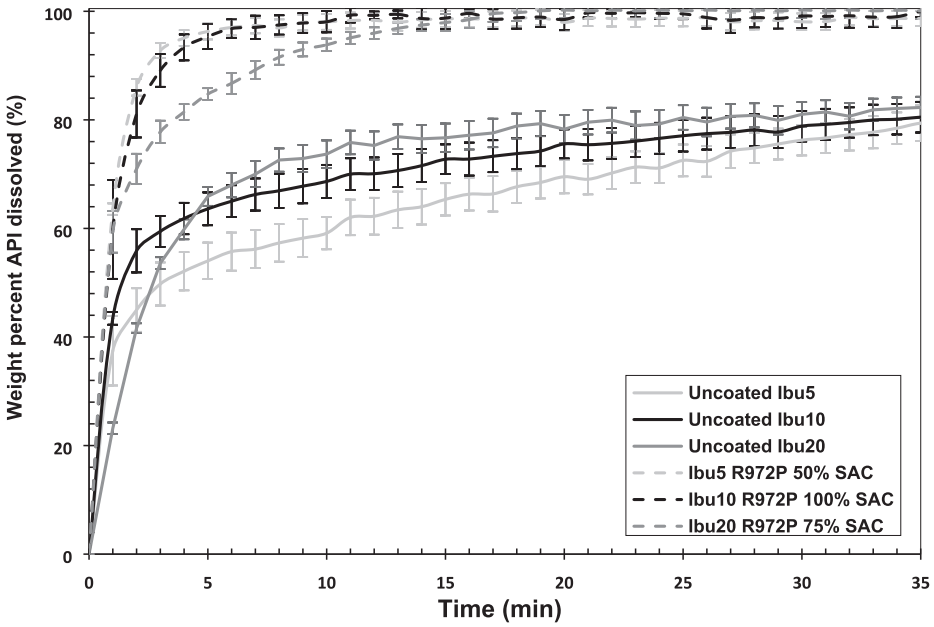

Fig. 13. Dissolution profiles for three fine APIs (Ibu20, Ibu10, Ibu5), uncoated or dry coated with hydrophobic silica shown at % SAC that resulted in the highest dissolution performance during 35 min of dissolution. The dissolution testing was done using USP IV flow-through-cell method with SDS 12 mM solution as the dissolution medium.

density. Both these outcomes, while positive and welcome, test conventional wisdom regarding powder behavior and point to the need for additional work. One area of such work is to examine the synergy due to the mixing process when one of the ingredients is dry coated. Another area is to investigate if the dry coated ingredient must be an API. If improved drug dissolution and drug content uniformity are important objectives, it makes sense that the dry coated constituent needs to be the API since fine API agglomeration is significantly mitigated by dry coating as shown in *Section 3.2*. However, if the DC processability is the main objective, one may consider dry coating of the excipient instead of the API. In the remainder of this sub-section, exemplary outcomes for excipient dry coating, also called excipient engineering, are presented first, followed by an investigation of low drug loaded blends with dry coated APIs to assess the enhancement in FFC and drug content uniformity.

In a trend-setting work, it was shown that dry coating can lead to the development of fine engineered excipients that have simultaneously improved three desirable qualities in an excipient; flowability, bulk density, and compaction [10,12,13,53]. Most remarkable outcome was that dry coated fine Avicel PH105 could promote DC processability for three different fine APIs, mAPAP, cAPAP, and IBU50, at drug loadings of as high as 60 wt%, suggesting a possibility that such engineered excipient may be used when API dry coating is not possible or not advisable. Exemplary results, shown in Fig. 14(b) [12], demonstrate that all three blends of IBU50 and cAPAP are DC capable, whereas, for mAPAP, although the 10 wt% blend meets the bar and the 30 wt% blend nearly meets the bar, the 60 wt% blend cannot meet the bar, hence for very fine APIs at high drug loading, dry coating of the API may be necessary. An important research question is if popular commercially available excipients designed for DC formulations such as silicified MCCs could achieve performance as good as dry coated Avicel PH105 for mAPAP binary blends. Interestingly, as shown in Fig. 14(c) [12], at each drug loading, dry coated mAPAP outperformed both Prosolv 90 and Prosolv 50. None of those excipients could enable DC at API loading of 30 or 60 wt%. Such outcomes suggest additional work is needed to gain an understanding of such complex behavior of powder blends and possible synergy of using finer ingredients when one of the constituents is dry coated.

Next, DC processability at very low drug loading is considered. An earlier work [9], although not targeting DC processability, examined improved blend uniformity of the binary blends of mAPAP and Avicel PH-102 and concluded that excellent drug content uniformity (CU) was achieved for 3, 5 and 10 wt% API loaded blends when mAPAP was dry coated. Motivated by such outcomes, a recent work examined DC processability in addition to enhanced CU [62]. Multi-component blends of fine excipients with fine milled API (IBU10 $\sim$ 10 μm) were considered at 1, 3, and 5 wt% drug loadings. As an unanticipated, surprising outcome, blends exhibited profound enhancement in flowability and bulk density at such low API loadings, as well as the CU for even the lowest drug loading [62]. Exemplary results for the processability, indicated via the blend FFC and agglomeration ratio (AR) are shown in Fig. 15(a) for 1 and 5 wt% drug loadings. Since both the API and excipients are fine (note the placebo blend FFC-AR in the figure), it is not surprising that the blend FFC values with uncoated API powder indicate the blends are *cohesive*, and blend AR is high. Remarkably, however, with dry coated API with either A200 or R972P silica, both blends with low drug loading achieved FFC of 6.8 or higher, suggesting DC processability. The reason why this is surprising and suggests an existence of synergy during the blending process is that the total amount of silica in these blends is minute and as low as 0.007 wt%. Such FFC enhancement seems to be extraordinary since such a low amount of added silica (not dry coated onto the API) during blending could not achieve flow enhancement [62]. Along with the enhanced FFC, dry coating also enabled low relative standard deviation (RSD) indicating enhanced CU for these blends as shown in Fig. 15(b). As was observed before [9], to achieve better CU at very low drug loading, it is not necessarily beneficial to have 100 % silica SAC, which is also the case here, since CU is better for 50 % SAC for 1 wt% drug loading. These results point to the need for more extensive research answering the question of how much silica is really necessary and how the potential transfer of silica from the dry coated component to other uncoated components during blending could lead to synergistic enhancements in blend properties.

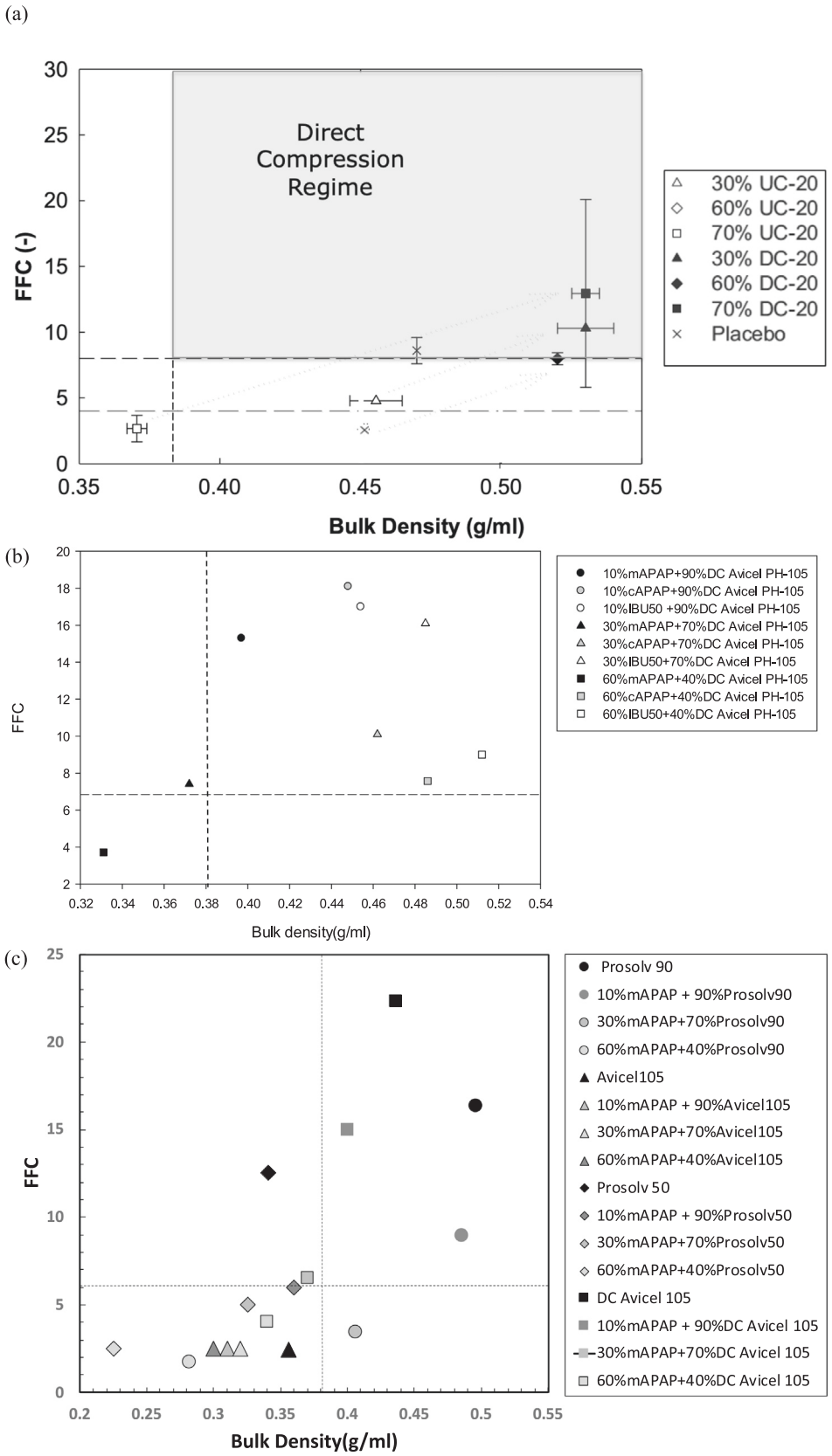

Fig. 14. Bulk density and FFC phase maps for selected formulations. (a) Formulations with coarse excipients for three drug loadings (30, 50, 70 wt%), with or without dry coating of micronized ibuprofen (IBU20). (b) Binary formulations of three different fine APIs at 10, 30, and 60 wt% drug loading with dry coated fine excipient (Avicel pH 105). (b) Binary formulations of mAPAP at three drug loadings (10, 30, 60 wt%) with Avicel pH 105 with or without dry coating as well as two size grades of commercial silicified excipients.

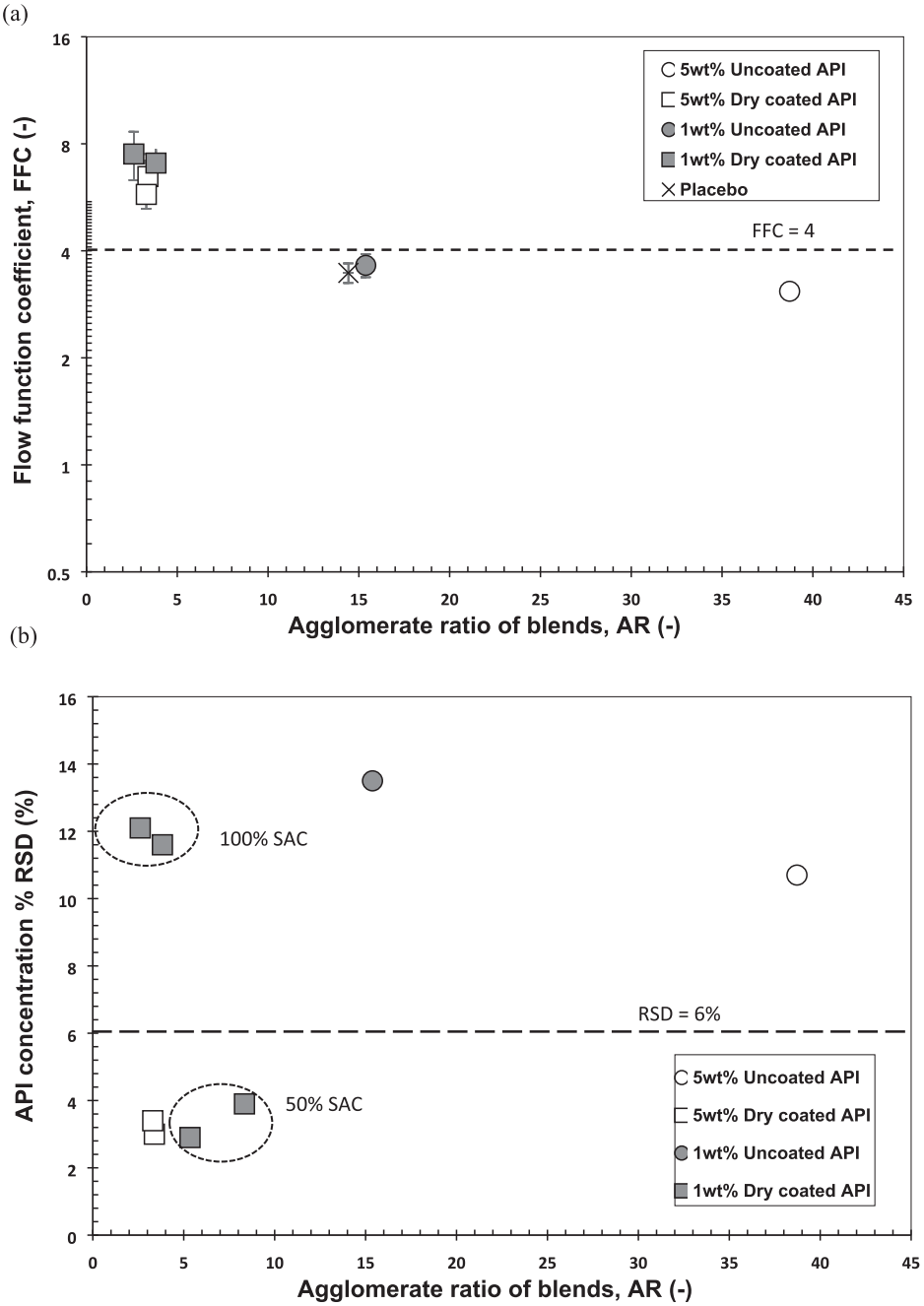

Fig. 15. Synergy between the dry coating and mixing low API loaded multi-component blends. For each drug load, either A200 or R972P were used for dry coating the API. (a) significant improvement in the bulk powder flow (FFC) with reduced blend agglomerate ratio (AR), (b) notably improved blend uniformity with the reduced AR when the silica amount was reduced from 100 % SAC to 50 % SAC.

4. Summary and future work/forward outlook

Model-guided dry coating-based enhancement of poor flow, packing, and dispersibility of fine cohesive powders having high cohesion was presented. Scrutiny of particle-contact models revealed that particle surface roughness has a predominant effect, which is significantly greater than the effect from particle surface energy. Hence the nearly *optimal* separation of the particles due to the nano-scale surface roughness superimposed by nano-coating was the main mechanism of flow enhancement through dry coating. Analysis of the existing models indicated that Chen-NJCEP model can better account for multi-asperity contacts and the extent of silica SAC. Models for determination of the amount and type of silica was presented, followed by the procedure to nondimensionalize cohesion through granular Bond number, which could be estimated via particle-scale measures; characteristic particle size, particle (true) density, asperity size, SAC %, and dispersive surface energy.

Key examples were presented to demonstrate the use of dry coating for mitigating problems of flow, packing, agglomeration, and dissolution of pharmaceutical powders. The impact of dry coating on powder agglomeration, an important yet often overlooked bulk property, was analyzed. As a novelty, AR was shown to be a screening indicator of the powder flowability, bulk density,

and dissolution; the lower the AR, the better the flow, higher the packing, and faster the dissolution. Most interestingly, dissolution was faster even with hydrophobic silica coating, indicating the dominating influence of reduced AR. Several illustrative case studies of blends having one dry coated component were presented to highlight the advantages of dry coating that extend well beyond improved properties of an individual powder. As a major novelty, enhanced flowability and improved drug content uniformity due to mixing synergy were observed even for a very low amount of silica in the blend, when a minor component was dry coated, e.g., fine API at 1 or 5 wt% drug loading. When it is not feasible to dry coat an API powder, the formulation could use fine, dry coated engineered excipients for enhanced DC processability at relatively high drug loadings.

It is hoped that the analysis and results presented in this paper point to the importance of dry coating as a useful tool for industry practitioners across disciplines. The models and guidelines for implementation should facilitate the use of dry coating at the lab-scale and provide sufficient information to make decisions regarding its relevance to commercial usage. Notwithstanding this positive forward outlook, several challenges, as well as opportunities remain.

- ***Modeling***: Enhancements of particle contact models to account for particle morphology, shape, surface roughness, improved methods for accurate prediction of the guest amounts, higher-intensity device relevant prediction of host–guest compatibility, the effect of guest particle agglomeration, and, incorporating full particle size distributions (PSDs), or mixed PSDs arising from multi-modal blend constituents for nondimensionalization of cohesion.
- ***Characterization***: Developing reliable, simpler methods to assess the magnitude and distribution of natural surface asperities, assessing the extent of silica transfer during blending, robust algorithms to accurately measure actual SAC, material sparing measures to assess the extent of cohesion reduction, instruments for *in situ* assessment of the dry coating process endpoint.
- ***Processing***: Develop robust process models and guidelines for (1) appropriate selection of processing parameters and estimating the needed process time, (2) lab-scale transferability from material sparing testing using devices like LabRAM to continuous scalable devices such as comil or fluid energy mill (FEM), and (3) scale-up rules.

Declaration of Competing Interest

The authors declare that they have no known competing financial interests or personal relationships that could have appeared to influence the work reported in this paper.

Acknowledgements

The authors are grateful for significant contributions to this topic by the past and current students from the lead author's group, Yuhua Chen, Laila Jallo, Xi Han, Maxx Capece, Xiaoliang Deng, Zhonghui Huang, Liang Chen, Kai Zheng, and Zhixing Lin. Generous donations and contributions of materials and characterization instruments are acknowledged from Aveka, BASF, Evonik, Freeman Technology, FMC Biopolymer, Gamlen, Mallinckrodt, and Surface Measurement Systems.

Funding

Financial support for the research covered in this paper over the past dozen years from National Science Foundation (NSF) grants EEC-0540855, IIP- 1537197, IIP- 1919037, and IIP- 2137209 is gratefully acknowledged. The lead author is thankful for the Fulbright-Nehru Academic and Professional Excellence Senior Research Scholar support, and a grant from the International Fine Particle Research Institute (IFPRI).

References

[1] X. Han, C. Ghoroi, D. To, Y. Chen, R. Davé, Simultaneous micronization and surface modification for improvement of flow and dissolution of drug particles, Int. J. Pharm. 415 (2011) 185–195.
[2] M.P. Mullarney, L.E. Beach, R.N. Davé, B.A. Langdon, M. Polizzi, D.O. Blackwood, Applying dry powder coatings to pharmaceutical powders using a comil for improving powder flow and bulk density, Powder Technol. 212 (2011) 397–402.
[3] L. Beach, J. Ropero, A. Mujumdar, M. Alcalà, R.J. Romañach, R.N. Davé, Near-infrared spectroscopy for the in-line characterization of powder voiding part II: Quantification of enhanced flow properties of surface modified active pharmaceutical ingredients, J. Pharmaceut. Innovat. 5 (2010) 1–13.
[4] L.J. Jallo, C. Ghoroi, L. Gurumurthy, U. Patel, R.N. Davé, Improvement of flow and bulk density of pharmaceutical powders using surface modification, Int. J. Pharm. 423 (2012) 213–225.
[5] C. Ghoroi, L. Gurumurthy, D.J. McDaniel, L.J. Jallo, R.N. Davé, Multi-faceted characterization of pharmaceutical powders to discern the influence of surface modification, Powder Technol. 236 (2013) 63–74.
[6] X. Han, C. Ghoroi, R. Davé, Dry coating of micronized API powders for improved dissolution of directly compacted tablets with high drug loading, Int. J. Pharm. 442 (2013) 74–85.
[7] Z. Huang, J.V. Scicolone, X. Han, R.N. Davé, Improved blend and tablet properties of fine pharmaceutical powders via dry particle coating, Int. J. Pharm. 478 (2015) 447–455.
[8] Z. Huang, J.V. Scicolone, L. Gurumuthy, R.N. Davé, Flow and bulk density enhancements of pharmaceutical powders using a conical screen mill: a continuous dry coating device, Chem. Eng. Sci. 125 (2015) 209–224.
[9] Z. Huang, W. Xiong, K. Kunnath, S. Bhaumik, R.N. Davé, Improving blend content uniformity via dry particle coating of micronized drug powders, Eur. J. Pharm. Sci. 104 (2017) 344–355.
[10] L. Chen, X. Ding, Z. He, Z. Huang, K.T. Kunnath, K. Zheng, R.N. Davé, Surface engineered excipients: I. improved functional properties of fine grade microcrystalline cellulose, Int. J. Pharm. (2018) 127–137.
[11] Z. Huang, K.T. Kunnath, X. Han, X. Deng, L. Chen, R.N. Davé, Ultra-fine dispersible powders coated with L-Leucine via two-step co-milling, Adv. Powder Technol. 29 (2018) 2957–2965.
[12] L. Chen, Z. He, K.T. Kunnath, S. Fan, Y. Wei, X. Ding, K. Zheng, R.N. Davé, Surface engineered excipients: III. Facilitating direct compaction tableting of binary blends containing fine cohesive poorly-compactable APIs, Int. J. Pharmaceut. 557 (2019) 354–365.
[13] L. Chen, Z. He, K. Kunnath, K. Zheng, S. Kim, R.N. Davé, Fine grade engineered microcrystalline cellulose excipients for direct compaction: Assessing suitability of different dry coating processes, Eur. J. Pharm. Sci. 151 (2020).
[14] K. Kunnath, L. Chen, K. Zheng, R.N. Davé, Assessing predictability of packing porosity and bulk density enhancements after dry coating of pharmaceutical powders, Powder Technol. 377 (2021) 709–722.
[15] N. Varun, A. Dutta, C. Ghoroi, Influence of surface interaction between drug and excipient in binary mixture for dry powder inhaler applications, Adv. Powder Technol. 33 (2022).
[16] K. Dixit, V. Karde, A. Jauhari, S.C. Bhattacharyya, C. Ghoroi, Flow improvement of fine oxidizer using nano-additives, Adv. Powder Technol. 33 (2022).
[17] J.G. Osorio, K. Sowrirajan, F.J. Muzzio, Effect of resonant acoustic mixing on pharmaceutical powder blends and tablets, Adv. Powder Technol. 27 (2016) 1141–1148.
[18] D. Schulze, J. Schwedes, J.W. Carson, Powders and bulk solids: Behavior, characterization, storage and flow, 2008.
[19] K. Thalberg, D. Lindholm, A. Axelsson, Comparison of different flowability tests for powders for inhalation, Powder Technol. 146 (2004) 206–213.

[20] L.J. Jallo, M. Schoenitz, E.L. Dreizin, R.N. Dave, C.E. Johnson, The effect of surface modification of aluminum powder on its flowability, combustion and reactivity, Powder Technol. 204 (2010) 63–70.
[21] M. Capece, Z. Huang, D. To, M. Aloia, C. Muchira, R.N. Davé, A.B. Yu, Prediction of porosity from particle scale interactions: Surface modification of fine cohesive powders, Powder Technol. 254 (2014) 103–113.
[22] T. Yano, S. Ohsaki, H. Nakamura, S. Watano, Numerical study on compression processes of cohesive bimodal particles and their packing structure, Adv. Powder Technol. 32 (2021) 1362–1368.
[23] F. Podczeck, Y. Miah, The influence of particle size and shape on the angle of internal friction and the flow factor of unlubricated and lubricated powders, Int. J. Pharm. 144 (1996) 187–194.
[24] L.J. Jallo, Y. Chen, J. Bowen, F. Etzler, R. Dave, Prediction of inter-particle adhesion force from surface energy and surface roughness, J. Adhes. Sci. Technol. 25 (2011) 367–384.
[25] U.V. Shah, D. Olusanmi, A.S. Narang, M.A. Hussain, J.F. Gamble, M.J. Tobyn, J.Y. Y. Heng, Effect of crystal habits on the surface energy and cohesion of crystalline powders, Int. J. Pharm. 472 (2014) 140–147.
[26] J.F. Gamble, W.S. Chiu, M. Tobyn, Investigation into the impact of sub-populations of agglomerates on the particle size distribution and flow properties of conventional microcrystalline cellulose grades, Pharm. Dev. Technol. 16 (2011) 542–548.
[27] S.T. Nase, W.L. Vargas, A.A. Abatan, J.J. McCarthy, Discrete characterization tools for cohesive granular material, Powder Technol. 116 (2001) 214–223.
[28] A.B. Yu, C.L. Feng, R.P. Zou, R.Y. Yang, On the relationship between porosity and interparticle forces, Powder Technol. 130 (2003) 70–76.
[29] A. Castellanos, The relationship between attractive interparticle forces and bulk behaviour in dry and uncharged fine powders, Adv. Phys. 54 (2005) 263–376.
[30] V. Boonkanokwong, J.G. Khinast, B.J. Glasser, Scale-up and flow behavior of cohesive granular material in a four-bladed mixer: effect of system and particle size, Adv. Powder Technol. 32 (2021) 4481–4495.
[31] L. Massimilla, G. Donsì, Cohesive forces between particles of fluid-bed catalysts, Powder Technol. 15 (1976) 253–260.
[32] J. Yang, A. Sliva, A. Banerjee, R.N. Dave, R. Pfeffer, Dry particle coating for improving the flowability of cohesive powders, Powder Technol. 158 (2005) 21–33.
[33] Y. Chen, J. Yang, R.N. Dave, R. Pfeffer, Fluidization of coated group C powders, AIChE J. 54 (2008) 104–121.
[34] S. Kim, E. Bilgili, R.N. Davé, Impact of altered hydrophobicity and reduced agglomeration on dissolution of micronized poorly water-soluble drug powders after dry coating, Int. J. Pharm. 606 (2021).
[35] H. Rumpf, Die Wissenschaft des Agglomerierens, Chem. Ing. Tech. 46 (1974) 1.
[36] H.Y. Xie, The role of interparticle forces in the fluidization of fine particles, Powder Technol. 94 (1997) 99–108.
[37] R. Mei, H. Shang, J.F. Klausner, E. Kallman, A contact model for the effect of particle coating on improving the flowability of cohesive powders, Kona Powder Part. J. 15 (1997) 132–141.
[38] Y.I. Rabinovich, J.J. Adler, A. Ata, R.K. Singh, B.M. Moudgil, Adhesion between nanoscale rough surfaces. I. Role of asperity geometry, J. Colloid Interface Sci. 232 (2000) 10–16.
[39] H. Krupp, Particle adhesion theory and experiment, Adv. Colloid Interface Sci. 1 (1967) 111–239.
[40] S. Bhattacharjee, C.H. Ko, M. Elimelech, DLVO interaction between rough surfaces, Langmuir 14 (1998) 3365–3375.
[41] C.Q. LaMarche, S. Leadley, P. Liu, K.M. Kellogg, C.M. Hrenya, Method of quantifying surface roughness for accurate adhesive force predictions, Chem. Eng. Sci. 158 (2017) 140–153.
[42] K. Cooper, N. Ohler, A. Gupta, S. Beaudoin, Analysis of contact interactions between a rough deformable colloid and a smooth substrate, J. Colloid Interface Sci. 222 (2000) 63–74.
[43] Y. Chen, M.A.S. Quintanilla, J. Yang, J.M. Valverde, R.N. Dave, Pull-off force of coated fine powders under small consolidation, Phys. Rev. E – Statist. Nonlinear Soft Matter Phys. 79 (2009).
[44] Y. Chen, L. Jallo, M.A.S. Quintanilla, R. Dave, Characterization of particle and bulk level cohesion reduction of surface modified fine aluminum powders, Colloids Surf., A 361 (2010) 66–80.
[45] J.A. Greenwood, J.B.P. Williamson, Contact of nominally flat surfaces, Proceedings of the Royal Society of London (1966) 19.
[46] B. Bhushan, Contact mechanics of rough surfaces in tribology: single asperity contact, Appl. Mech. Rev. 49 (1996) 275–298.
[47] B. Bhushan, Contact mechanics of rough surfaces in tribology: multiple asperity contact, Tribol. Lett. 4 (1998) 1–35.
[48] J. Larsson, S. Biwa, B. Storåkers, Inelastic flattening of rough surfaces, Mech. Mater. 31 (1999) 29–41.
[49] G.G. Adams, M. Nosonovsky, Contact modeling - forces, Tribol. Int. 33 (2000) 431–442.
[50] B.N.J. Persson, Capillary adhesion between elastic solids with randomly rough surfaces, J. Phys.: Condens. Matter 20 (2008).
[51] C. Ghoroi, X. Han, D. To, L. Jallo, L. Gurumurthy, R.N. Davé, Dispersion of fine and ultrafine powders through surface modification and rapid expansion, Chem. Eng. Sci. 85 (2013) 11–24.
[52] K. Kunnath, Z. Huang, L. Chen, K. Zheng, R. Davé, Improved properties of fine active pharmaceutical ingredient powder blends and tablets at high drug loading via dry particle coating, Int. J. Pharm. 543 (2018) 288–299.
[53] L. Chen, X. Ding, Z. He, S. Fan, K.T. Kunnath, K. Zheng, R.N. Davé, Surface engineered excipients: II. Simultaneous milling and dry coating for preparation of fine-grade microcrystalline cellulose with enhanced properties, Int. J. Pharmaceut. 546 (2018b) 125-136.
[54] H. Egermann, I. Kemptner, E. Pichler, Effects of interparticulate interactions on mixing homogeneity, Drug Dev. Ind. Pharm. 11 (1985) 663–676.
[55] C.Y. Huang, M.S. Ku, Asymmetry effect of particle size distribution on content uniformity and over-potency risk in low-dose solid drugs, J. Pharm. Sci. 99 (2010) 4351–4362.
[56] A.L. Bowler, S. Bakalis, N.J. Watson, A review of in-line and on-line measurement techniques to monitor industrial mixing processes, Chem. Eng. Res. Des. 153 (2020) 463–495.
[57] S. Eichenlaub, A. Gelb, S. Beaudoin, Roughness models for particle adhesion, J. Colloid Interface Sci. 280 (2004) 289–298.
[58] Y. Johno, M. Satomi, K. Nakashima, T. Shigematsu, B. Ono, Numerical simulation of particle settling and cohesion in liquid, J. Phys. Conf. Ser. 147 (2009).
[59] J.N. Israelachvili, Intermolecular and surface forces: revised, third edition., Academic press, 2011.
[60] L.J. Jallo, R.N. Dave, Explaining electrostatic charging and flow of surface-modified acetaminophen powders as a function of relative humidity through surface energetics, J. Pharm. Sci. 104 (2015) 2225–2232.
[61] X. Han, L. Jallo, D. To, C. Ghoroi, R. Davé, Passivation of high-surface-energy sites of milled ibuprofen crystals via dry coating for reduced cohesion and improved flowability, J. Pharm. Sci. 102 (2013) 2282–2296.
[62] S.S. Kim, C. Castillo, M. Sayedahmed, R.N. Dave, Reduced fine API agglomeration after dry coating for enhanced blend uniformity and processability of low drug loaded blends Pharmaceutical Research (2022b). Published online, https://doi.org/10.1007/s11095-022-03343-6.
[63] X. Deng, R.N. Davé, Adhesion and friction of dry-coated nano-rough particles, Powder Technol. 314 (2017) 20–27.
[64] K. Zheng, K. Kunnath, Z. Ling, L. Chen, R.N. Davé, Influence of guest and host particle sizes on dry coating effectiveness: when not to use high mixing intensity, Powder Technol. 366 (2020) 150–163.
[65] R. Dave, W. Chen, A. Mujumdar, W. Wang, R. Pfeffer, Numerical simulation of dry particle coating processes by the discrete element method, in: Adv. Powd. Technol. 2003:449–470.
[66] X. Deng, Z. Huang, W. Wang, R.N. Davé, Investigation of nanoparticle agglomerates properties using Monte Carlo simulations, Adv. Powder Technol. 27 (2016) 1971–1979.
[67] S. Wu, Polar and non-polar interactions in adhesion, J. Adhes. 5 (1973) 16.
[68] S. Kim, M. Cheikhali, R.N. Dave, Decoding fine API agglomeration as a key indicator of powder flowability and dissolution: Impact of particle engineering Pharmaceutical Research, (2022a). Published online, https://doi.org/10.1007/s11095-022-03293-z
[69] A.W. Jenike, Storage and flow of solids, in, Bulletin No. 123 of the Utah Engineering Experimental Station, Univerity of Utah, Salt Lake City, 1964.
[70] J. Schwedes, D. Schulze, Measurement of flow properties of bulk solids, Powder Technol. 61 (1990) 59–68.
[71] D. Schulze, Powders and Bulk Solids: Behavior, Characterization, Storage and Flow Springer: Berlin/Heidelberg, Germany, Heidelberg; New York; Tokyo, 2021.
[72] R. Freeman, Measuring the flow properties of consolidated, conditioned and aerated powders – a comparative study using a powder rheometer and a rotational shear cell, Powder Technol. 174 (2007) 25–33.
[73] W. Chen, R.N. Dave, R. Pfeffer, O. Walton, Numerical simulation of Mechanofusion system, Powder Technol. 146 (2004) 121–136.
[74] E. Hoashi, S. Yoshihashi-Suzuki, H. Nanba, T. Kanemura, H. Kondo, T. Furukawa, N. Yamaoka, H. Horiike, Numerical study on free surface flow of liquid metal lithium for IFMIF, Fusion Eng. Des. (2013) 2515–2519.
[75] H. Honda, T. Matsuno, M. Koishi, Preparation of a graphite fluoride modified-polymer microsphere by a high speed impact treatment method, J. Soc. Powder Technol. Japan 25 (1988) 5.
[76] H. Honda, T. Matsuno, M. Koishi, The effect of powder properties on dry impact blending preparation method, J. Soc. Powder Technol. Japan 25 (1989) 5.
[77] H. Honda, K. Ono, T. Ishizak, T. Matsuno, M. Katano, M. Koishi, Surface modification of powders by the high speed impact treatment method, J. Soc. Powder Technol. Japan 24 (1987) 6.
[78] M. Yang, H. Yamamoto, H. Kursashima, H. Takeuchi, H. Yokoyama, H. Tsujimoto, Y. Kawashima, Design and evaluation of poly(dl-lactic-co-glycolic acid) nanocomposite particles containing salmon calcitonin for inhalation, Eur. J. Pharm. Sci. 46 (2012) 6.
[79] T. Ishizaka, H. Honda, M. Koishi, Drug dissolution from indomethacin-starch hybrid powders prepared by the dry impact blending method, J. Pharm. Pharmacol. 45 (1993) 4.
[80] T. Yokoyama, K. Urayama, M. Naito, M. Kato, T. Yokoyama, The Angmill mechanofusion system and its applications, Kona Powder Part. J. 5 (1987) 59–68.
[81] M. Ramlakhan, C.Y. Wu, S. Watano, R.N. Dave, R. Pfeffer, Dry particle coating using magnetically assisted impaction coating: modification of surface properties and optimization of system and operating parameters, Powder Technol. 112 (2000) 137–148.
[82] Z. Huang, J.V. Scicolone, L. Gurumuthy, R.N. Davé, Flow and bulk density enhancements of pharmaceutical powders using a conical screen mill: a continuous dry coating device, Chem. Eng. Sci. (2014).

[83] S. Chattoraj, C.C. Sun, Crystal and particle engineering strategies for improving powder compression and flow properties to enable continuous tablet manufacturing by direct compression, J. Pharm. Sci. 107 (2018) 968–974.
[84] X. Deng, K. Zheng, R.N. Davé, Discrete element method based analysis of mixing and collision dynamics in adhesive mixing process, Chem. Eng. Sci. 190 (2018) 220–231.
[85] D. To, R.N. Davé, Fluid bed film coating of fine ibuprofen particles, Powder Technol. 290 (2016) 102–113.
[86] Y. Chen, J. Yang, R.N. Dave, R. Pfeffer, Granulation of cohesive Geldart group C powders in a Mini-Glatt fluidized bed by pre-coating with nanoparticles, Powder Technol. 191 (2009) 206–217.
[87] Y. Chen, J. Yang, A. Mujumdar, R. Dave, Fluidized bed film coating of cohesive Geldart group C powders, Powder Technol. 189 (2009) 466–480.
[88] V. Boonkanokwong, R.P. Frank, P. Valliappan, B. Remy, J.G. Khinast, B.J. Glasser, Flow of granular materials in a bladed mixer: Effect of particle properties and process parameters on impeller torque and power consumption, Adv. Powder Technol. 29 (2018) 2733–2752.
[89] A.A. Noyes, W.R. Whitney, The rate of solution of solid substances in their own solutions, J. Am. Chem. Soc. 19 (1897) 930–934.
[90] M.M. De Villiers, Influence of agglomeration of cohesive particles on the dissolution behaviour of furosemide powder, Int. J. Pharm. 136 (1996) 175–179.
[91] C.C. Sun, Setting the bar for powder flow properties in successful high speed tableting, Powder Technol. 201 (2010) 106–108.